3. EXPLANATORY NOTES[1]

Shipboard Scientific Party[2]

INTRODUCTION

This chapter outlines methods used to obtain and process data collected by Leg 150 participants. Methods used by various investigators for shore-based analyses of Leg 150 data will be described in the individual scientific contributions to be published in the *Scientific Results* volume.

Authorship of Site Chapters

The separate sections of the site chapters were written by the following shipboard scientists (authors are listed in alphabetical order, no seniority is implied):

Site Summary: Miller, Mountain
Background and Objectives: Miller, Mountain
Operations: Blum, Foss
Lithostratigraphy: Damuth, Deconinck, Hesselbo, Kotake, McCracken, McHugh, Saito, ten Kate
Biostratigraphy: Aubry, Burckle, Christensen, de Verteuil, Gartner, Katz, Snyder
Paleomagnetism: Urbat, van Fossen
Sedimentation Rates: Aubry, Christensen, Miller
Organic Geochemistry: Quayle
Inorganic Geochemistry: Compton
Physical Properties: Fulthorpe, Hoppie, Lorenzo, Vecsei
APC Downhole Temperature (ADARA): Blum
Downhole Measurements: Alm, Guerin
Seismic Stratigraphy: Miller, Mountain
Summary and Conclusions: Miller, Mountain

Summary core descriptions ("barrel sheets") and photographs of each core are included in Section 3. Downhole log measurements prepared onshore by the Borehole Research Group appear at the end of each site chapter.

The Ocean Drilling Program (ODP) is in the process of replacing the bulk of the "Explanatory Notes" chapters in each *Initial Reports* volume with a chapter entitled "Annual Explanatory Notes to *Initial Reports* Volumes." These complete, detailed, and annually updated notes will reduce redundancy and help keep the printing costs of the *Initial Reports* at reasonable levels. In anticipation of this change, we have omitted some of the general information that has been reprinted repeatedly in past *Initial Reports* volumes; where appropriate, reference is made to other *Initial Reports* volumes for detailed descriptions of methods.

Drilling Operations

Three coring systems were used during Leg 150: the advanced hydraulic piston corer (APC), the extended core barrel (XCB), and the rotary core barrel (RCB). Any one of these systems was applied to maximize core recovery in the lithology being drilled. Drilling systems and their characteristics, such as drilling-related deformation, are eloquently summarized in the "Explanatory Notes" chapter of the Leg 139 *Initial Reports* volume, and various versions are found in all previous volumes.

Shipboard Scientific Procedures

Numbering of sites, holes, cores, and samples followed standard ODP procedures. A full identification number for a sample consists of the following information: leg, site, hole, core number, core type, section number, piece number (for hard rock), and interval in centimeters measured from the top of the section. For example, a sample identification of "150-903A-10H-1, 10–12 cm" would be interpreted as representing a sample removed from the interval between 10 and 12 cm below the top of Section 1, Core 10 ("H" designates that this core was taken during hydraulic piston coring) of Hole 903A during Leg 150.

Cored intervals are referred to in meters below seafloor (mbsf); these are determined by subtracting the rig floor height above sea level (as determined at each site) from the drill-pipe measurements from the drill floor. Note that this measurement usually differs from precision depth recorder (PDR) measurements by a few to several meters (see Chapter 4, this volume).

General core handling procedures are described in previous *Initial Reports* volumes and the *Shipboard Scientists Handbook*, and are summarized here. As soon as cores arrived on deck, core-catcher samples were taken for the biostratigraphic laboratory, and gas void samples were taken with a vacutainer for immediate analysis as part of the shipboard safety and pollution prevention program. When the core was cut in sections, whole-round samples were taken for shipboard interstitial-water examinations and, from some cores, for shore-based consolidation tests. In addition, headspace gas samples were immediately scraped from the ends of cut sections and sealed in glass vials for light hydrocarbon analysis.

After we allowed the core to equilibrate for a minimum of 4 hr on deck, we ran whole-round sections through the Multisensor Track (MST; see "Physical Properties" section, this chapter) and performed thermal conductivity measurements. The cores were then split into working and archive halves. Cores were split from the bottom to top, so investigators should be aware that older material could have been transported upward on the split face of each section. The working half of each core was sampled for both shipboard and shore-based laboratory studies, whereas the archive half was described visually and by means of smear slide examination. Where needed and possible, thin sections were taken from the working half. Most archive sections were run through the cryogenic magnetometer. The archive half was then photographed with both black-and-white and color film, a whole core at a time, and close-up photographs (black-and-white) were taken of particular features for illustration in the summary of each site, as requested by individual scientists.

Both halves of the core were then put into labeled plastic tubes, sealed, and transferred to cold storage space aboard the drilling vessel. At the end of the leg, in St. John's, the cores were transferred from the ship into refrigerated vans that went by means of sea freight to Norfolk, Virginia, and then by truck to cold storage at the East Coast

Table 1. Lithologic unit boundaries, Leg 150.

Hole, core, section, interval (cm)	Unit or subunit	Depth to base of unit (mbsf)
902C-16H-1, 113	I	122.1
	No Unit II	
902C-19X-1, 50	III	152.5
902D-33X-CC, 40	IVA	293.0
902D-45X-1, 150	IVB	403.7
902D-60X-3, 90	VA	549.4
902D-65X-1, 108	VB	594.8
902D-74X-1, 74	VI	680.9
TD	VII	741.0
903B-16H-7, 87	IA	15.0
903A-32X-4, 45	IB	273.9
903A-36X-CC, 45	IIA	307.5
903A-41X-3, 20	IIB	358.9
903A-58X-2, 150	III	522.9
903A-68X-6, 112	IVA	624.6
903C-16R-5, 5	IVB	733.1
903C-41R-5, 90	V	974.4
903C-51X-CC, 21	V1	1064.1
TD	VII	1149.7
904A-12H-2, 65	I	106.2
	No Unit II or III	
904A-18H-CC, 18	IVA	167.8
904A-25X-2, 35	IVB	223.9
904A-32X-5, 140	V	296.5
904A-37X-4, 20	VI	341.2
904A-45X-3, 150	VIIA	418.9
TD	VIIB	576.7
905A-25H-CC, 30	I	215.0
905A-60X-5, 13	II	536.8
905A-75X-4, 114	III	679.8
TD	IV	910.6
906A-5H-4, 130	IA	43.3
906A-7H-2, 90	IB	55.4
	No Unit II or III	
906A-17X-6, 150	IVA	157.4
906A-30X-3, 135	IVB	279.2
906A-38X-CC, 35	VA	361.8
906A-45X-2, 33	VB	421.1
906A-51X-1, 101	VC	478.2
906A-59X-CC, 40	VI	555.3
TD	VII	602.4

Note: TD = total depth

Repository of the Ocean Drilling Program (at Lamont-Doherty Earth Observatory, Columbia University, New York).

LITHOSTRATIGRAPHY

The first part of this section summarizes the methods used to describe sediment cores and the procedure followed to condense these data into computer-generated summary sheets for each core using the ODP "Visual Core Description" (VCD) program. The second part reviews the sedimentological classifications and terms used in the descriptions. A third part describes the X-ray diffraction methods used to analyze the mineralogy of the sediments. Lithologic units and subunits at the five sites (902–906) drilled during Leg 150 were recognized on the basis of primary compositional and fabric characteristics (Table 1).

Visual Core Descriptions and the Barrel Sheet Program

Sedimentologists aboard Leg 150 were responsible for visual core descriptions (VCDs), smear-slide analyses, and thin-section descriptions of all cored sediment. Information recorded manually, section by section, on VCD sheets was condensed and entered into the "VCD" program, a graphical barrel sheet. The following is a summary of the Leg 150 use of the "VCD" program.

The lithology of the recovered material was depicted on the computer-generated core description forms by symbols representing up to three components in the column titled "Graphic Lith." (Fig. 1). Where an interval of sediment or sedimentary rock was a mixture of lithologic components, the constituent categories were separated by a solid vertical line, with each category represented by its own symbol. Constituents accounting for less than 10% of the sediment in a given lithology (or others remaining after the representation of the three most abundant lithologies) were not shown in the graphic lithology column, but were listed in the "Lithologic Description" section of the core description form. In intervals of thinly interbedded sediments comprising two or more lithologies of different compositions, the constituent categories were separated by a dashed vertical line. Because of the limited scale of the core summaries and the limits of the VCD program, the graphic lithology column shows only the composition of layers or intervals exceeding 16 cm in thickness.

The chronostratigraphic unit, as recognized on the basis of paleontologic and paleomagnetic criteria was recorded in the "Age" column on the core summaries. Boundaries between assigned ages were indicated as follows:

1. sharp boundary: straight line;
2. unconformity or hiatus: line with + signs above it; and
3. uncertain: line with question marks.

The "Structure" column was used to indicate, in addition to primary sedimentary structures, a wide variety of modifications to the sediment, such as soft-sediment deformation, and structural and diagenetic features (Fig. 2). On Leg 150, the shipboard sedimentologists decided to use the color-banding symbols to indicate both color banding and interbedded lithologies, because the latter were invariably accompanied by color changes. The following definitions were adopted from Blatt et al. (1980, p. 128):

thick bedding/color banding = >30 cm,
medium bedding/color banding = 10–30 cm, and
thin bedding/color banding = <10 cm

To simplify classification of the degree of bioturbation, a modified version of the terminology of Droser and Bottjer (1991) was used (Fig. 3). Interpretation of homogenous sediment presented problems. Leg 150 sedimentologists recognized that homogeneous sediment may be the product of primary deposition of material of homogeneous color and grain size, or the product of total mixing by the action of bioturbating organisms.

Deformation and disturbances of sediment that clearly resulted from the coring process were illustrated in the "Drilling Disturbances" column (using the symbols shown in Fig. 2). Blank regions indicate the absence of drilling disturbance. The degree of drilling disturbance was described for soft and firm sediments using the following categories:

1. slightly deformed: bedding contacts were slightly bent;
2. moderately deformed: bedding contacts were extremely bowed;
3. highly deformed: bedding was completely disturbed and in some places showed symmetrical diapir-like or flow structures; and
4. soupy: intervals were water saturated and had lost all aspects of original bedding.

The degree of fracturing in indurated sediments was described using the following categories:

1. slightly fractured: core pieces were in place and contained little drilling slurry or breccia;
2. moderately fragmented: core pieces were in place or partly displaced, but the original orientation was preserved or recognizable (drilling slurry may surround fragments);
3. highly fragmented: pieces were from the cored interval and probably in the correct stratigraphic sequence (although they may not represent the entire section), but the original orientation was completely lost; and

4. drilling breccia: core pieces have lost their original orientation and stratigraphic position and may have been mixed with drilling slurry.

The hue and chroma attributes of color were recorded in the "Color" column and were determined using Munsell Soil Color Charts (1971). A Minolta Spectrophotometer CM-2002 was available, but it was not used for the following reasons. The precision figures given for color values using this instrument (e.g., 8.8YR 5.7/3.7) are difficult to relate to the Munsell Soil Color Charts. Recording these in the "VCD" program would have required significant rounding up or down of the values, thus making only limited use of the precision of the instrument. Therefore, Leg 150 sedimentologists found the use of the color charts more compatible with the present version of the "VCD" program. The Minolta Spectrophotometer CM-2002 was also found to give highly variable readings across a core that to the human eye appeared homogeneous in color, suggesting that it is more sensitive than the human eye.

The location of all samples taken for shipboard analysis was indicated in the "Samples" column on the core description form, as follows:

C: organic-geochemistry sample,
D: XRD sample,
I: interstitial-water sample,
M: micropaleontology sample,
P: physical-properties sample,
S: smear slide,
T: thin section, and
X: paleomagnetic sample.

A figure summarizing key data from smear slides appears in each site chapter, and all data derived from smear-slide and thin-section analyses appear in Sections 4 and 5 (this volume). Included in these sections is information on the sample location, whether the sample represents a dominant ("D") or a minor ("M") lithology in the core, and the estimated percentages of sand-, silt-, and clay-size material, together with all identified components. One sample per core was analyzed for percentage of $CaCO_3$ and total organic carbon (see "Organic Geochemistry" section, this chapter). These data are presented in the "Organic Geochemistry" section for each site.

The lithologic description that appears on each core description form consists of three parts:

1. a heading that lists all the major sediment lithologies observed in the core;
2. a heading for minor lithologies; and
3. a more detailed description of these sediments, including features such as color, composition (determined from the analysis of smear slides), sedimentary structures, or other notable characteristics.

Descriptions and locations of thin, interbedded, or minor lithologies that could not be depicted in the graphic lithology column were included in the text.

Classification of Sediments and Sedimentary Rocks

Sedimentologists used the sediment classification scheme of the Ocean Drilling Program (Mazzullo et al., 1988) to describe the granular sediments drilled on Leg 150. Variations in the relative proportions of siliciclastic, volcaniclastic, pelagic, and neritic components define five major classes of granular sediments (Fig. 4). The pelagic component consists of the skeletal remains of open-marine siliceous and calcareous microfauna and microflora and the neritic component consists of reworked shallow-water microfauna and microflora and terrigenous and authigenic (e.g., glauconite) material. On Leg 150, no volcaniclastic material was recorded. Calcium carbonate content was qualitatively estimated using smear slides and quantitatively esti-
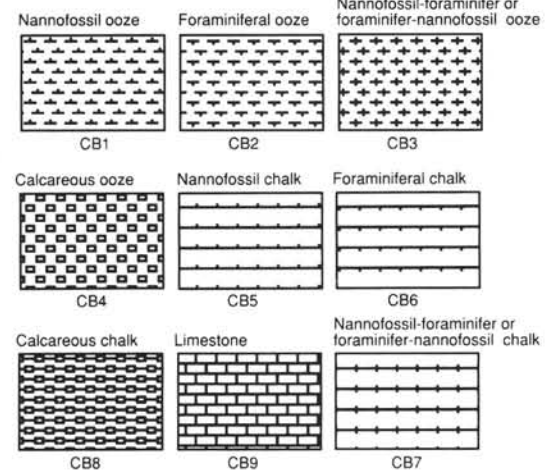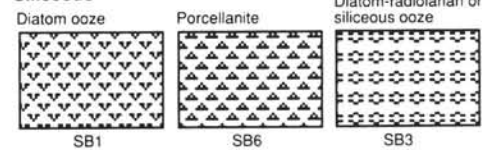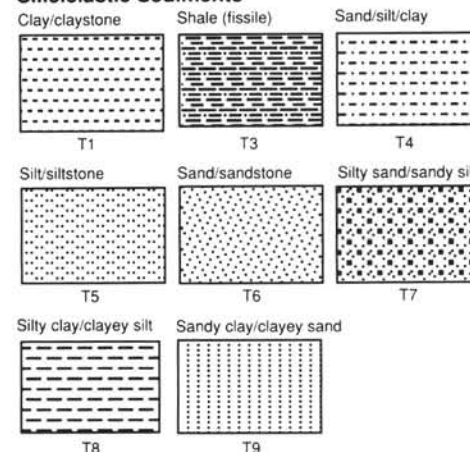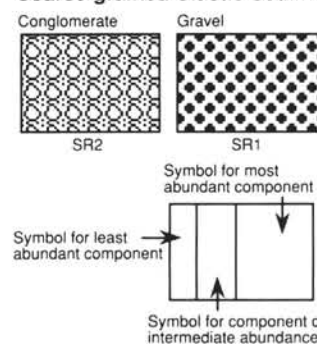
Figure 1. Key to symbols used in the "Graphic Lith." column on the computer-generated core description forms shown in Section 3 of this volume and in the generalized summary lithologic columns within the "Lithostratigraphy" sections of each site chapter.

Structure Symbols

⊿	Cross stratification	|<|	Vein
↑ F	Upward-fining sequence	-//	Injection
↑ C	Upward-coarsening sequence	⫯	Water-escape structure
≡	Parallel laminae	◆	Isolated mud clast
⌐	Cross-laminated	◆	Lithoclast
⊥⊥	Cross-bedded	◇	Isolated pebbles/cobbles
...	Graded bedding normal	⫽	Microfault, normal
⌁	Scoured contact with graded bed	⫽	Microfault, thrust
⚬⚬⚬	Convolute/contorted bedding	⌒	Slump blocks, slump folds
⌁⌁	Current ripples	⌔	Shell complete
ℰ	Contorted slump	✄	Shell fragments
▽	Scour	⟿	Wood fragment
	Sharp contact	⬠	Echinoderms
---	Gradational contact	⌂	Fish debris
⌄⌄	Scoured contact	⟓	Gastropods
≡	Thin color bands (sharp contact)	⟏	Bivalve
≋	Thin color bands (gradual contact)	⟑	*"Sagarites"*
▤	Laminations (millimeter scale)	⊕	Solitary coral
■	Individual thick color band	}	Slight bioturbation
▬	Individual medium color band	}}	Moderate bioturbation
▬	Individual thin color band	}}}	Heavy bioturbation
		⟫⟫	Discrete *Zoophycos* trace fossil

Drilling Deformation Symbols

⊙	Concretions/nodules	
(Ca)	Calcite nodule/concretion	
Ca	Calcite disseminated	
(C)	Carbonate nodule/concretion	
C	Carbonate disseminated	
(P)	Pyrite nodule/concretion	
p	Pyrite disseminated	
(G)	Glauconite	

Soft sediments:

	Slightly disturbed
	Moderately disturbed
⟳	Very disturbed
ooo	Soupy

Hard sediments:

///	Slightly fractured
⊥⊥	Moderately fractured
>>	Highly fractured
xxx	Drilling breccia

Figure 2. Symbols used for sedimentary structures, components, and drilling disturbance on the computer-generated core description forms shown in Section 3 of this volume.

mated by coulometric analyses (see "Organic Geochemistry" section, this chapter, for method).

A granular sediment was classified by designating a principal name and major and minor modifiers. The principal name of a granular sediment (e.g., ooze, fine sand, or sandstone) defines its granular sediment class, as depicted in Figure 4; the major and minor modifiers describe the texture, composition, and fabric.

For siliciclastic sediments, the principal name describes the texture and was assigned according to the following guidelines:

1. The Udden-Wentworth grain-size scale (Wentworth, 1922) defines grain-size ranges and names of the textural groups (gravel, sand, mud) and subgroups (fine sand, coarse silt, etc.) that were used as the principal names of siliciclastic sediment.

2. Principal names were listed in order of increasing abundance when two or more textural groups or subgroups were present in a siliciclastic sediment (Shepard, 1954; Fig. 4). For simplicity, we grouped intermediate mixtures of the three textural end-members (i.e., sand, silt, and clay) into the four categories shown in Figure 5.

3. The suffix "-stone" was affixed to the principal names sand, silt, and clay when the sediments were lithified. The degree of lithifi-

cation was described using the following major modifiers: "unlithified" designates soft sediment that was readily deformable by finger pressure, "partially lithified" designates firm sediment that was incompletely lithified, and "lithified" designates hard, cemented sediment that had to be cut with a saw.

For pelagic sediment, the principal name describes the composition and degree of lithification using the following terms:

1. ooze: unlithified calcareous and/or siliceous pelagic sediments.
2. chalk: partially lithified sediment predominantly composed of calcareous pelagic grains.
3. radiolarite, diatomite, and spiculite: partially lithified sediment predominantly composed of siliceous radiolarians, diatoms, and sponge spicules, respectively.
4. porcellanite: a well-indurated rock with greater than 50% authigenic silica but less hard, lustrous, or brittle than chert.

The principal name of a granular-sediment class is preceded by major modifiers and followed by minor modifiers (the latter preceded by "with") that describe the lithology of the granular sediment in
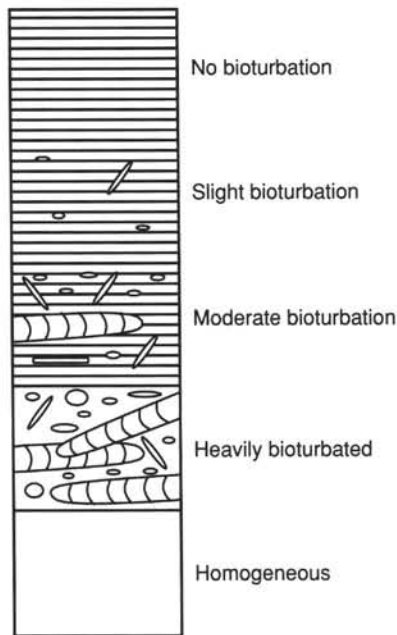
Figure 3. Nomenclature used to classify degree of bioturbation (modified from Droser and Bottjer, 1991).

Figure 4. Diagram showing classes of granular sediment (from Mazzullo et al., 1988).

greater detail (e.g., a siliciclastic rock composed of 50% clay, 35% quartz-silt, and 15% foraminifers is classified as a silty claystone with foraminifers). Major and minor modifiers, as applied in the previous example, were used most commonly to describe composition and textures of grain types present in major (>25%) and minor (10%–25%) proportions. Major and minor modifiers were also used to describe grain fabric (e.g., matrix supported) in siliciclastic sediment types.

The composition of bioclastic grains was described with the major and minor modifiers diatom(-aceous), radiolarian, siliceous, nannofossil, foraminifer(-al), and calcareous. The terms "siliceous" and "calcareous" were used generally to describe sediments composed of siliceous or calcareous pelagic grains.

Grain shape, mineralogy, rock-fragment types, fabric, degree of induration, and color were used as major modifiers. Grain shapes were described by the major modifiers as rounded, subrounded, subangular, and angular. The character of siliciclastic grains was described by mineralogy (using modifiers such as "quartzose," "glauconitic," "micaceous," or "calcareous"). The fabric of a sediment was described using major modifiers such as "grain-supported," "matrix-supported," and "imbricated." Generally, fabric terms were useful only when describing gravels and conglomerates. Finally, sediment color, as determined visually with the Munsell Color Chart (1971), was also employed as a major modifier. Mixed sediments were described using major and minor modifiers indicating composition and texture.

X-ray Diffraction

The mineralogy of sediments was determined using the shipboard Philips PW 1729 X-ray diffractometer with CuKα radiation (Ni filter). Instrument conditions were as follows; 40 KV, 35 mA, goniometer scan from 2° to 70°, step size 0.01°, count time 0.5 s. Bulk sediments were freeze-dried, crushed, and mounted in random orientation in aluminum sample holders. Peaks were visually inspected according to the Mineral powder diffraction file (McClune, 1983) and occasionally matched to standard reference peaks for various minerals. The relative distribution of the identified minerals is plotted according to the intensity of their main diffraction peak intensity (quartz = 3.34Å, feldspars = 3.2Å–3.25Å, calcite = 3.03Å, dolomite
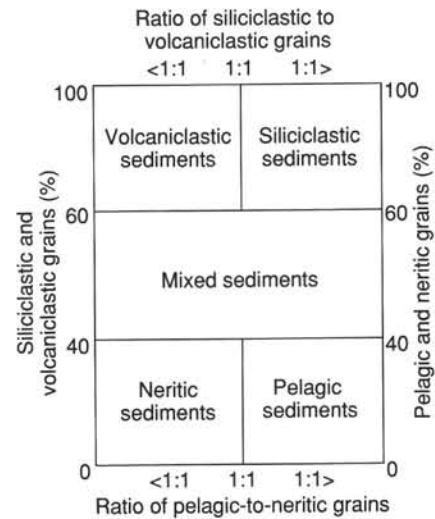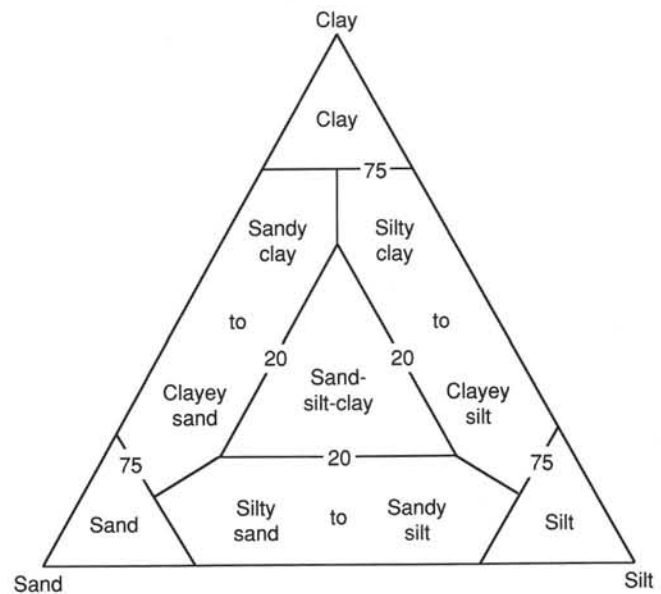
Figure 5. Ternary diagram showing principal names for siliciclastic sediments (modified from Shepard, 1954).

= 2.89Å, pyrite = 2.71Å, siderite = 2.8Å, opal A = very broad peak around 4Å, and opal CT = peak near 4.1Å; Kastner, 1981).

BIOSTRATIGRAPHY

Preliminary age assignments were established using core-catcher samples. Samples from elsewhere in the cores were examined when a more refined age determination was necessary and when time permitted. Four microfossil groups were examined for biostratigraphic purposes: calcareous nannofossils, planktonic foraminifers, diatoms, and dinoflagellate cysts (dinocysts). Benthic foraminifers were used to estimate paleobathymetry and to determine in situ from transported biofacies. Sample positions and the abundance, preservation, and chronostratigraphic age or biozone for each fossil group were recorded on barrel sheets for each core. The Neogene time scale used in this work was from Berggren, Kent, and van Couvering (1985; noted in the site
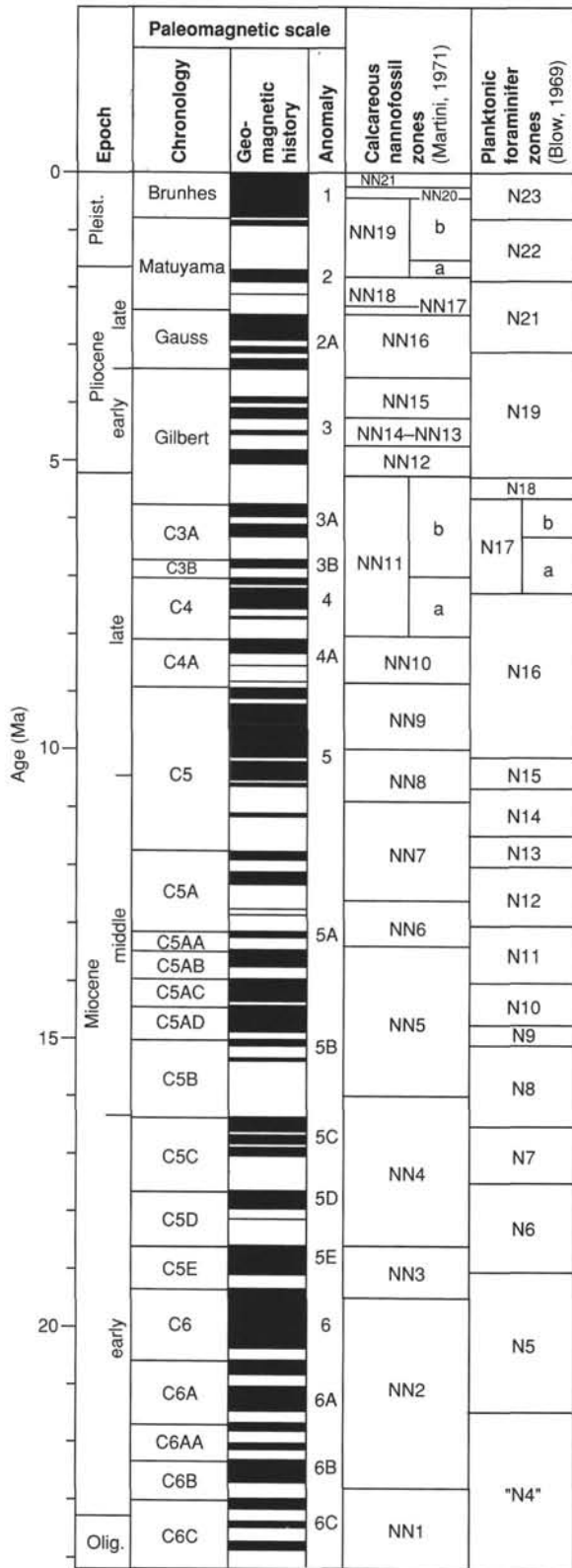
Figure 6. Correlation of the Neogene chronostratigraphy, biostratigraphy, and magnetostratigraphy used during Leg 150. Correlation of the magnetic polarity record and the epoch boundaries follows that of Berggren, Kent, and van Couvering (1985). Estimated numerical ages of zonal indicators can be found in Tables 2 and 3.

Table 2. Cenozoic calcareous nannofossil datums used for Leg 150.

Event		Calibration	Age (Ma)	Zone (base)
BA	*Emiliania huxleyi*		0.085	
B	*Emiliania huxleyi*		0.26	NN21
T	*Pseudoemiliania lacunosa*		0.46	NN20
T	*Helicosphaera sellii*		1.12	
T	*Calcidiscus macintyrei (cir., >10 µm)*		1.54	
B	*Gephyrocapsa oceanica >4.0 µm*		1.58	
B	*Gephyrocapsa caribbeanica*		1.64	
T	*Discoaster brouweri*	Olduvai	1.81	NN19
T	*Discoaster pentaradiatus*	Matuyama	2.27	NN18
T	*Discoaster surculus*		2.40	NN17
T	*Discoaster tamalis*	Gauss	2.60	
T	*Sphenolithus abies/neoabies*	Gilbert	3.45	
T	*Reticulofenestra pseudoumbilicus*	Gilbert	3.56	NN16
B	*Discoaster tamalis*		3.80	
BA	*Discoaster asymmetricus*	Gilbert	3.87	
TA	*R. pseudoumbilicus/Sphenolithus abies*		4.10	
B	*Pseudoemiliania lacunosa*		4.00	
T	*Amaurolithus tricorniculatus*		4.26	NN15
T	*Ceratolithus acutus*	Sidufjall	4.43	
B	*Ceratolithus rugosus*	Thvera	4.90	NN13
B	*Ceratolithus acutus*	Gilbert	5.17	
B	*Triquetrorhabdulus rugosus*	Gilbert	5.30	
T	*Amaurolithus primus*		5.54	
T	*Discoaster quinqueramus*	Gilbert	5.38	NN12
T	*Amaurolithus amplificus*	C3A	6.01	
B	*Amaurolithus amplificus*	C3A	6.34	
B	*Amaurolithus primus*	C3A/C4	7.01	NN11
B	*Discoaster quinqueramus*	C4	7.60	
B	*Discoaster berggrenii*	C4	8.28	NN11
T	*Discoaster bollii*		8.38	
T	*Discoaster hamatus*	C4A	8.85	NN10
T	*Catinaster spp.*	C4A	9.00	
B	*Discoaster hamatus*	C5	10.0	NN9
B	*Catinaster calyculus*	C5	10.0	
T	*Coccolithus miopelagicus*	C5	10.22	
B	*Catinaster coalitus*		11.5	NN8
T	*Cyclicargolithus floridanus*		11.71	
B	*Discoaster kugleri*	C5A	12.2	NN7
B	*Triquetrorhabdulus rugosus*	C5A	12.5	
T	*Sphenolithus heteromorphus*	C5AB	13.37	NN6
T	*Helicosphaera ampliaperta*	C5B	16.00	NN5
TA	*Discoaster deflandrei*	C5B	16.05	
B	*Sphenolithus heteromorphus*	C5D	18.42	
T	*Sphenolithus belemnos*	C5E	18.8	NN4
B	*Sphenolithus belemnos*	C6	19.4	
T	*Triquetrorhabdulus carinatus*			NN3
B	*Discoaster druggii*	C6C	22.8	NN2
TA	*Sphenolithus delphix*		22.8	
T	*Reticulofenestra bisecta*		23.3	
A	*Sphenolithus delphix*		24.5	
T	*Sphenolithus ciperoensis*	C6C/C7	24.6	
T	*Helicosphaera recta*	C6C	24.7	NN1
T	*Sphenolithus distentus*	C9	27.6	NP25
B	*Sphenolithus ciperoensis*	C10	29.4	NP24
B	*Sphenolithus distentus*		33.1	
T	*Reticulofenestra umbilicus*	C12	33.7	NP23
T	*Ericsonia formosa*	C12	34.0	NP22
T	*Discoaster saipanensis*	C13	35.6	NN21
T	*Discoaster barbadiensis*	C13	35.6	
B	*Isthmolithus recurvus*	C15	37.1	NP19
B	*Chiasmolithus oamaruensis*	C16	38.4	NP18
T	*Chiasmolithus solitus*	C18	40.8	NP17
B	*Nannotetrina alata*	C21	48.1	NP15
B	*Discoaster sublodoensis*	C22	50.8	NP14
B	*Discoaster lodoensis*	C23	54.0	NP12

Notes: T = top, B = bottom, BA = bottom acme, and TA = top acme. Ages are from Berggren et al. (1985a, 1985c), and Gartner (1990).

chapters as BKV85). The Paleogene time scale was from Berggren, Kent, and Flynn (1985; noted in the site chapters as BKF85) and Aubry et al. (1988) (Figs. 6–7). Tables 2 and 3 summarize the microfossil datum levels, respectively, used for Leg 150, and Table 4 provides the series and series subdivisions based on microfossil data.

Calcareous Nannofossils

Cenozoic Zonation

We have referred primarily to the zonation and code number of Martini (1971). Whenever possible, we applied the subzonal criteria

Table 3. Cenozoic planktonic foraminifer datums used for Leg 150.

	Event	Age (Ma)	Zone (base)
T	*Globigerinoides fistulosus*	1.6	
T	*Globigerinoides obliquus extremus*	1.8	
B	*Globorotalia truncatulinoides*	1.9	N22
T	*Globoquadrina altispira*	2.9	
B	*Globigerinoides fistulosus*	2.9	
T	*Sphaeroidinellopsis* spp.	3.0	N21
B	*Globorotalia tosaensis*	3.1	
T	*Pulleniatina primalis*	3.5	
T	*"Globigerina" nepenthes*	3.9	
B	*Globorotalia crassaformis*	4.3	
B	*Sphaeroidinella dehiscens*	5.1	N19
B	*Globorotalia tumida*	5.2	N18
B	*Globigerinoides conglobatus*	5.3	
T	*Globoquadrina dehiscens*	5.3	
B	*Pulleniatina primalis*	5.8	
B	*Neogloboquadrina humerosa*	7.5	N17
B	*Globorotalia plesiotumida*	—	
B	*Neogloboquadrina acostaensis*	10.2	N16
T	*Globorotalia siakensis*	10.4	N15
B	*"Globigerina" nepenthes*	11.3	N14
B	*Sphaeroidinellopsis subdehiscens*	11.8	N13
B	*Globorotalia fohsi lobata*	13.1	
B	*Globorotalia praefohsi*	13.9	N11
B	*Globorotalia peripheroacuta*	14.9	N10
B	*Orbulina suturalis*	15.2	N9
B	*Praeorbulina sicana*	16.6	N8
T	*Catapsydrax dissimilis*	17.6	N7
B	*Globigerinatella insueta*	—	N6
T	*Globorotalia kugleri*	21.8	N5
B	*Globoquadrina dehiscens*	23.2	
B	*Globorotalia kugleri*	23.7	"N4"
B	*Globigerinoides primordius*	25.8	
T	*Paragloborotalia opima*	28.2	P22
T	*Globigerina ampliapertura*	32.8	P21
T	*Pseudohastigerina*	34.0	P20
T	hantkeninids, *Globigerinatheka*	36.6	P18
B	*Globigerina tapuriensis*	36.6	
T	*Turborotalia cerroazulensis* group	36.6	
T	*Cribrohantkenina inflata*	37.3	P17
B	*Cribrohantkenina inflata*	38.0	P16
T	*Acarinina*	40.6	P15
T	*Morozovella spinulosa*	41.1	
B	*Globigerinatheka semiinvoluta*	41.3	
T	*Globigerinatheka beckmanni*	42.6	P14
B	*Globigerapsis beckmanni*	42.7	P13
T	*Morozovella aragonensis*	46.0	P12
B	*Globigerapsis kugleri*	48.1	P11
B	*Hantkenina*	52.0	P10
B	*Planorotalites palmerae*	53.4	P9
T	*Morozovella formosa*	53.7	P8
B	*Morozovella aragonensis*	55.2	P7
B	*Morozovella formosa*	56.1	P6c

Notes: T = top, and B = bottom. Ages are from Berggren et al. (1985a, 1985c), and Berggren and Miller (1988).

defined by Bukry (1973, 1975) and codified by Okada and Bukry (1980) and Gartner (1977, 1990). Primary and secondary biostratigraphic event zonal markers for the Cenozoic are shown in Table 2 and Figure 7.

Methods

Calcareous nannofossil assemblages were described from smear slides prepared for each core-catcher sample and for as many samples in between as time permitted. Intervals with low sedimentation rates or with suspected unconformities were sampled as closely as was practical. Turbidites and slumps were sampled in the hemipelagic and pelagic intervals and special attention was given to lithologic changes. Examination was done exclusively with a light microscope, using whatever optical configuration yielded useful results. In all cases, a magnification of ×1250 was used to estimate the semiquantitative abundance.

Abundances of individual species were estimated for each sample. Five levels of abundance were recorded, with the following approximate definitions:
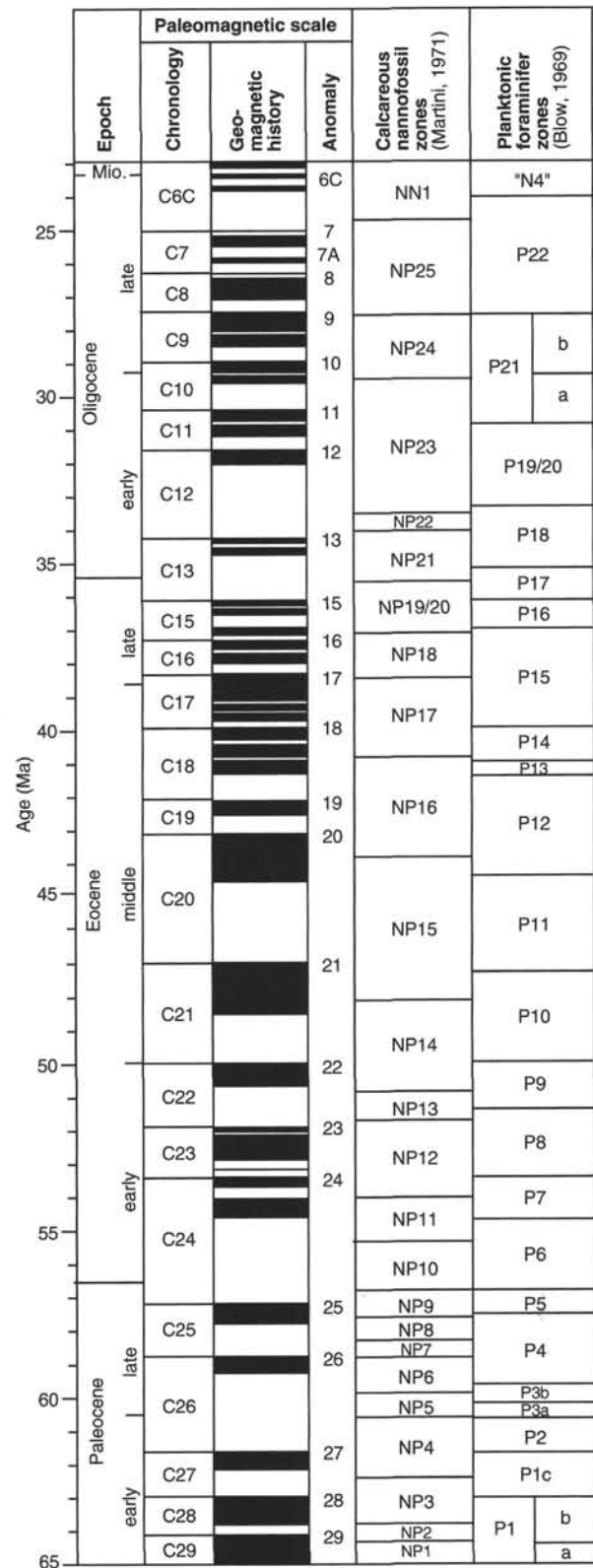
Figure 7. Correlation of the Paleogene chronostratigraphy, biostratigraphy, and magnetostratigraphy used during Leg 150. Correlation of the magnetic polarity record and the epoch boundaries follows that of Berggren, Kent, and Flynn (1985). Estimated numerical ages of zonal indicators can be found in Tables 2 and 3.

Table 4. Chronostratigraphic boundaries, Leg 150.

Hole	Depth (mbsf)	
902A	1	Holocene
902C	122.1	middle-upper Pleistocene
902D	267.59	upper Miocene
902D	564.6 or 536.0	middle Miocene
902D	611	lower Miocene
902D	680.9	upper to uppermost lower Oligocene
902D	to TD	upper Eocene
903A	0.2	Holocene
903A	350	middle-upper Pleistocene
903A	352	Pliocene
903C	510	upper Miocene
903D	919.25	middle Miocene
903C	998.8	lower Miocene
903C	1064.12	upper Oligocene
903C	1115	upper Eocene
903C	to TD	middle Eocene
904A	4.27	Holocene
904A	106.2	middle-upper Pleistocene
904A	148.61 or 181.35	upper Miocene
904A	245.75	middle Miocene
904A	313.45	lower Miocene
904A	341.2	upper Oligocene
904A	418.9	upper Eocene
904A	561.8	middle Eocene
904A	to TD	lower Eocene
905A	20	??
905A	218.7	lower Pleistocene
905A	218.7-231.36	upper Pliocene to lower Pleistocene
905A	303.2	Pliocene
905A	596.6	upper Miocene
905A	to TD	middle Miocene
906A	2.7	Holocene
906A	43.5	middle-upper Pleistocene
906A	91.5 or 168.98	upper Miocene
906A	478.2	middle Miocene
906A	555.5	upper Oligocene
906A	to TD	upper Eocene

V (very rare) = 1 specimen only;

R (rare) = 1 specimen per 51–200 fields of view (2–5 specimens total);

F (few) = 1 specimen per 11–50 fields of view (6–15 specimens total);

C (common) = 1 specimen per 2–10 fields of view (16–250 specimens total);

A (abundant) = 1–10 specimens per field of view (251–500 specimens total); and

W (very abundant) = more than 10 specimens per field of view (>500 specimens total).

The total abundance of calcareous nannofossils for each sample was estimated as follows:

B (barren);

R (rare) = 1–10 specimens for 500 fields of view (about three traverses);

F (few) = 11–50 specimens for 500 fields of view;

C (common) = 51–2000 specimens for 500 fields of view;

A (abundant) = 2001–20,000 specimens for 500 fields of view; and

W (very abundant) = >20,000 specimens for 500 fields of view.

The qualitative evaluation of the preservation of calcareous nannofossils was recorded as good (G), moderate (M), or poor (P). These categories represent subjective impressions with approximately the following meaning:

P (poor) = severe dissolution, fragmentation and/or overgrowth has occurred; primary features may have been destroyed, and many specimens cannot be identified at the species level;

M (moderate) = dissolution and/or overgrowth are evident; a significant proportion (as much as 25%) of the specimens cannot be confidently identified at the species level with absolute certainty; and

G (good) = little or no evidence of dissolution and/or overgrowth is present; diagnostic characteristics are preserved and nearly all specimens (about 95%) can be identified.

Foraminifers

Methods

Samples of approximately 20 cm^3 were soaked in a Calgon solution and washed through a 63-μm sieve. Samples were rinsed and then dried under a heat lamp.

Preservation characteristics were divided into three categories:

P (poor) = almost all specimens were dissolved or broken and fragments dominated;

M (moderate) = 30%–90% of specimens showed dissolved or broken chambers; and

G (good) = >90% of specimens were well preserved and unbroken.

Planktonic Foraminifers

The Cenozoic zonal scheme of Blow (1969, 1979) was employed, with slight modifications by Stainforth et al. (1975), Kennett and Srinivasan (1983), and Berggren, Kent, and van Couvering (1985) for the Neogene; by Bolli and Saunders (1985) for the Oligocene to Holocene; and by Toumarkine and Luterbacher (1985) and Berggren and Miller (1988) for the Paleogene. Zonal markers for biostratigraphic events during the Cenozoic are shown in Table 3.

The >125-μm fraction was examined for planktonic foraminifers and the 63- to 125-μm fraction was studied for zonal markers if these were absent in the larger size fractions.

The abundance of planktonic foraminifers is defined as follows:

B (barren);

R (rare) = <10 specimens;

F (few) = 10–100 specimens;

C (common) = 101–500 specimens; and

A (abundant) = >500 specimens.

Benthic Foraminifers

Benthic foraminifers were examined from the >150-μm size fraction. Paleobathymetry estimates were primarily based on Van Morkhoven et al. (1986). Bathymetric zones were defined as follows: the neritic (0–200 m) was divided into upper (0–30 m), middle (30–100 m), and lower (100–200 m) zones; the bathyal was divided into upper (200–600 m), middle (600–1000 m), and lower (1000–2000 m) zones; and the abyssal was divided into upper (2000–3000 m) and lower (>3000 m).

Benthic foraminifer relative abundance was defined qualitatively as follows:

B (barren);

R (rare) = <1% of the fauna;

C (common) = 1%–10% of the fauna; and

A (abundant) = >10% of the fauna.

Diatoms

Components from both near-shore and open-ocean environments were present in the diatom assemblages. Accordingly, our use of existing zonations reflect this fact; we used zonations that have been developed for the Atlantic coastal plain as well as the zonation for the North Atlantic. The coastal plain zonations of Andrews (1976, 1978, 1988) and Abbott (1978, 1980) were primarily used, but these were supplemented by the North Atlantic zonation scheme of Baldauf (1984, 1987). Although we encountered many species common in coastal plain sediments, the North Atlantic zonation is directly tied to other zonal schemes.

Methods

Diatom assemblages were described from smear slides prepared from each core-catcher sample and from as many samples in between as time permitted. Intervals with low sedimentation rates or with suspected unconformities were sampled as closely as was practical. Examination was done exclusively with a light microscope, using magnifications of ×400 to ×1000 to estimate the semiquantitative abundance.

Both total abundance and abundance of individual species were estimated for each sample. Five levels of abundance were recorded, with the following approximate definitions:

R (rare) = 1 specimen or species in more than 50 fields of view (2–5 specimens total);

F (few) = 1 specimen or species per 11–50 fields of view (6–15 specimens total);

C (common) = 1 specimen or species per 2–10 fields of view (16–250 specimens total);

A (abundant) = 1–10 specimens or species per field of view (251–500 specimens total).

The qualitative evaluation of the preservation of diatoms was recorded as good (G), moderate (M), or poor (P). These categories represent subjective impressions with approximately the following meaning:

P (poor) = severe dissolution and/or fragmentation has occurred; primary features destroyed and many specimens not identified at the species level;

M (moderate) = dissolution is evident; a significant proportion (as much as 25%) of the specimens cannot be identified to species with absolute certainty; and

G (good) = little or no evidence of dissolution is present; diagnostic characteristics are preserved and nearly all specimens (where at least one half of the valve is present) can be identified.

Dinoflagellates

Pliocene and Pleistocene age assignments are based largely upon detailed unpublished data from DSDP Site 603 (Kolev, 1993). These data are supplemented by other magnetostratigraphically constrained dinocyst datum levels from DSDP Sites 607 and 611 (Mudie, 1987). For the Miocene we have used the dinocyst zonation of de Verteuil and Norris (1991, 1992) that was developed for coeval sediments in Maryland, Virginia, and New Jersey. The zones are calibrated using dinocyst datum levels established for several sections in the North Atlantic and Europe (summarized in Head et al., 1989a). They are defined in de Verteuil and Norris (unpubl. data, 1993) and are summarized here:

Zone Pre-A: Interval from the highest occurrence of *Thalassiphora? pansa* Stover 1977 to the highest occurrence of *Chiropteridium* spp. Age is late early Oligocene to early early Miocene.

Zone A: Interval from the highest occurrence of *Chiropteridium* spp. to the highest occurrence of *Cordosphaeridium cantharellum* (Brosius) Gocht 1969. Age is middle early Miocene.

Zone B: Interval from the highest occurrence of *Cordosphaeridium cantharellum* (Brosius) Gocht 1969 to the lowest occurrence of *Labyrinthodinium truncatum* Piasecki 1980. Age is middle to late early Miocene.

Zone C: Interval from the lowest occurrence of *Labyrinthodinium truncatum* Piasecki 1980 to the highest occurrence of *Distatodinium paradoxum* (Brosius) Eaton 1976. Age is early middle Miocene.

Zone D: Interval from the highest occurrence of *Distatodinium paradoxum* (Brosius) Eaton 1976 to the highest occurrence of *Systematophora placacantha* (Deflandre and Cookson) Davey et al. 1969. Age is middle middle Miocene.

Zone E: Interval from the highest occurrence of *Systematophora placacantha* (Deflandre and Cookson) Davey et al. 1969 to the lowest

occurrence of *Cannosphaeropsis* sp. cf. *C. utinensis* (= *C. utinensis* sensu Brown and Downie, 1985). Age is middle middle Miocene.

Zone F: Interval from the lowest occurrence of *Cannosphaeropsis* sp. cf. *C. utinensis* (= *C. utinensis* sensu Brown and Downie, 1985) to the highest occurrence of *Cannosphaeropsis* sp. cf. *C. utinensis* (= *C. utinensis* sensu Brown and Downie, 1985). Age is late middle Miocene.

Zone G: Interval from the highest occurrence of *Cannosphaeropsis* sp. cf. *C. utinensis* (= *C. utinensis* sensu Brown and Downie, 1985) to the highest occurrence of *Sumatradinium soucouyantiae* de Verteuil and Norris 1992. Age is early late Miocene.

Zone H: Interval from the highest occurrence of *Sumatradinium soucouyantiae* de Verteuil and Norris 1992 to the highest occurrence of *Hystrichosphaeropsis obscura* Habib 1972. Age is middle late Miocene.

Zone I: Interval from the highest occurrence of *Hystrichosphaeropsis obscura* Habib 1972 to the highest occurrence of *Erymnodinium delectabile* (de Verteuil and Norris) Lentin et al. 1994. Age is late late Miocene.

The Oligocene biostratigraphy draws upon dinocyst events in several well-constrained studies, including Bujak et al. (1980), Biffi and Manum (1988), Head and Norris (1989), Brinkhuis (1992), and Brinkhuis et al. (1992). These are supplemented by the Northern Hemisphere composite range estimates of Williams et al. (1993) and by studies summarized in Head and Norris (1989).

Methods

As many 10-cm^3 core-catcher samples were examined as time permitted. Rarely, additional samples were examined from intervals of particular stratigraphic interest. Processing consisted of heating the sample in 1% Calgon solution, followed by sieving through a 25-µm Nitex nylon sieve. Residues were then digested in 20% hydrochloric acid and washed to neutrality. Because of the high silica contents, samples were macerated for 15–20 min in hot concentrated hydrofluoric acid and again washed to neutrality. This was followed by a second application of 20% hydrochloric acid in a hot bath to dissolve precipitated fluorides. Swirling the organic residues in a large watchglass removed residual silicates, sulfides, and detrital minerals when they were present. Residues were strew mounted in glycerine gel and examined in bright field-transmitted light.

Dinocyst floral lists are incomplete for most samples, and no attempts were made to estimate species abundances except to note where certain taxa clearly dominated any particular assemblage.

The qualitative evaluation of the preservation of dinocysts only was recorded as good (G), moderate (M), or poor (P). These categories represent subjective impressions with approximately the following meaning:

P (poor) = severe bacterial infestation and/or mechanical fragmentation has occurred; primary features destroyed and many specimens cannot be identified at the species level;

M (moderate) = bacterial infestation and/or mechanical fragmentation is evident; a significant proportion (up to 25%) of the specimens cannot be identified to species level with absolute certainty; and

G (good) = little or no evidence of bacterial infestation and/or mechanical fragmentation; diagnostic characteristics are preserved and nearly all specimens (about 95%) can be identified.

All assemblages recovered are thermally immature so that thermal alteration is not a relevant factor in fragmentation or color alteration of palynomorphs.

PALEOMAGNETISM

Paleomagnetic studies performed aboard *JOIDES Resolution* during Leg 150 included routine pass-through measurements of natural

remanent magnetization (NRM) and volume magnetic susceptibility (k) of recovered material. In general, the archive half was demagnetized in a 10- or 15-mT alternating field (AF) for the removal of any secondary magnetizations. As a guide to the pass-through data, thermal and AF demagnetization experiments were conducted on discrete samples from the working halves. Alternatively to the pass-through measurements, 5 to 7 samples per core from the working halves were demagnetized in progressively higher peak alternating fields of up to 90 mT. In addition, isothermal remanent magnetization (IRM and backfield IRM) acquisition experiments on discrete samples were used as an aid in determining the magnetic mineralogy of the cored material.

Laboratory Instruments

The paleomagnetic laboratory on *JOIDES Resolution* maintained two magnetometers for measurement of magnetic remanence during Leg 150: a pass-through cryogenic superconducting rock magnetometer manufactured by 2-G Enterprises (Model 760R) and a Molspin spinner magnetometer. An on-line AF demagnetizer, capable of 20 mT (2-G Model 2G600), included on the pass-through cryogenic magnetometer track for demagnetization of whole-core sections.

The sensing coils in the cryogenic magnetometer measure the signal over about a 20-cm interval, and the coils for each axis have slightly different response curves. The large volume of core material within the sensing region (200–300 cm^3) allows the measurement of remanence in weakly magnetized samples, despite the relatively high background noise related to the motion of the ship. The practical limit on the sensitivity seems to be imposed by the magnetization of the core liner itself (equivalent to a volume of sediment with a magnetization intensity of 0.1 mA/m). However, the smaller volume of discrete cube samples (6 cm^3) and the magnetization of the plastic cube tray requires a material of higher magnetization intensity to enhance the signal. Based on tests made during transit, we estimate this magnetization intensity to be about 1 mA/m. The pass-through cryogenic magnetometer and its AF demagnetizer are controlled by BASIC programs ("Cryosect" and "Cryocube," respectively) modified from the original SUPERMAG program that runs on a PC-AT-compatible computer.

The Molspin "Minispin" magnetometer was used for measuring remanent magnetizations in discrete samples. Samples were spun at 6 Hz within a ring fluxgate housed in triple-layer Mu metal shielding. The signal is integrated over 6 s (noise level ≥0.2 × 10^{-6} emu/cm^3) or 24 s (noise level ≥0.1 × 10^{-6} emu/cm^3). Declination, inclination, and magnetization intensity were calculated using either a three- or six-position spin routine, the latter of which permits calculation of a circular standard deviation. The "Minispin" was interfaced with a Macintosh SE/30 and controlled by a True Basic program. The laboratory has an alternating-field (AF) demagnetizer and a thermal demagnetizer (Models GSD-1 and TSD-1 by the Schonstedt Instrument Co.) capable of demagnetizing discrete specimens to 100 mT and 700°C, respectively.

The magnetic susceptibility of whole cores was measured with a Bartington Instruments magnetic susceptibility meter (Model MS1, adapted with a MS1/CX 80-mm whole-core sensor loop set at 0.465 kHz), mounted with the GRAPE and *P*-wave logger on the multisensor track (MST). The full width of the impulse response peak at half maximum is less than 5 cm. The low-field susceptibility of discrete specimens can be measured on board either with a dual-frequency sensor unit (type MS1B) attached to a Bartington MS2 susceptibility meter or a Kappabridge KLY-2 (Geofyzika Brno). The Kappabridge is a semiautomatic autobalance inductivity bridge with a high sensitivity (4 × 10^{-8} SI units) and an accuracy of ±0.1% within one measuring range, which can be used to determine the anisotropy of magnetic susceptibility (AMS) as well.

An Analytical Services Company (ASC) Model IM-10 impulse magnetizer was used for studies of stepwise acquisition of saturation isothermal remanence magnetization (sIRM) in discrete samples. For IRM studies, a subset of shipboard samples was subjected to a steady

magnetic field along the +Z axis and measured with the Molspin magnetometer. This process was repeated at progressively higher fields (as high as 1.2 T). The samples were then given a back-field IRM by applying progressively higher direct fields along the –Z axis up to one step beyond the measured remanent coercivity of the samples.

Core Orientation

During APC coring, full orientation was achieved with the new digital multishot tool (Tensor, Inc.) rigidly mounted onto a nonmagnetic sinker bar. The Tensor tool consists of three mutually perpendicular magnetic field sensors and two perpendicular gravity sensors. The information from both sets of sensors allows the azimuth and dip of the hole to be measured as well as the azimuth of the APC core double orientation line.

Remanent Magnetization Measurements

The NRM measurements of sediments and rocks were performed by passing continuous archive half-core sections in 10-cm intervals through the cryogenic magnetometer. The ODP core orientation scheme arbitrarily designates the positive *X*-axis direction as the horizontal (in situ) line radiating from the center of the core through the space between a double line scribed lengthwise on the working half of each core liner. The maximum AF demagnetizing field allowed by the Information Handling Panel for archive-half sections is 15 mT or the median destructive field, whichever is lower. In some cores, this field is insufficient to remove secondary remanence and isolate the primary component of remanence required for magnetostratigraphic and cruise objectives. Therefore, at least one discrete shipboard paleomagnetic sample was taken from each core and from each representative lithology. The discrete samples were either AF or thermally demagnetized in stepwise fashion using the Minispin or cryogenic magnetometer, respectively. Demagnetization data for the discrete samples were graphically analyzed using orthogonal demagnetization plots, and vector statistics were calculated using the method of Fisher (1953).

Discrete samples in soft sediment were taken using oriented standard plastic boxes (6 cm^3). To reduce the deformation of the sediment, the core was cut using a thin stainless steel spatula before pressing the plastic sampling boxes into the sediment.

Magnetostratigraphy

Where magnetic cleaning successfully isolates the primary component of remanence, paleomagnetic inclinations (and declinations for the APC cores) are used in conjunction with biostratigraphic data to establish a magnetic polarity stratigraphy for the cores. During Leg 150, we used the Cenozoic magnetobiostratigraphy of Berggren, Kent, Flynn, and van Couvering (1985; noted as BKFV85 in the site chapters) with the magnetic polarity geochronology and terminology of Cande and Kent (1992, noted as CK92 in the site chapters; see Table 5).

Low-field Susceptibility

Whole-core susceptibility measurements are relatively rapid to make, are nondestructive, and provide an indication of the amount of magnetizable material in the sediment, including ferrimagnetic and paramagnetic constituents. Whole-core volume magnetic susceptibility was measured on the automated multisensor track (MST) at both the low and high sensitivity ranges, at intervals determined by recovery, usually every 10 cm. The susceptibility meter was zeroed after each section, but no baseline drift corrections were applied on the ship. Because magnetic susceptibility is a temperature-dependent property, the cores were permitted to equilibrate thermally for about 4 hr before being analyzed. Susceptibility data were used to (1) char-

acterize relative changes in susceptibility downcore, (2) provide an auxiliary correlation tool among the Leg 150 sites, and (3) aid in the documentation of environmental and geologic changes recorded in the sediments.

INORGANIC GEOCHEMISTRY

Shipboard analyses were performed on interstitial waters extracted from 5- to 15-cm-long, whole-round sediment samples. Samples were taken from each core to a depth of 100 mbsf and from every third core at depths below 100 mbsf. The closer sampling interval of the upper 100 mbsf provided a better definition of the steepest portion of the interstitial-water gradients. The whole-round sections were cut from the core immediately after arrival on deck, and the surfaces of the samples were scraped with a Teflon-coated spatula to remove potentially contaminating sediment. Each sample was squeezed up to 40,000 lb in a titanium squeezer. Interstitial water was expressed into a plastic syringe and filtered through a 0.45-μm acrodisc filter. Shipboard samples were stored in plastic vials in a refrigerator pending analysis. Sample splits were sealed in glass ampules for ODP archives and for shore-based elemental analysis. Shore-based samples were acidified with Ultrex HCl.

Alkalinity and pH were determined in duplicate immediately following sample collection using the Metrohm autotitrator with a Brinkman combination pH electrode. The electrode was calibrated before the analyses and was checked periodically for drift. Salinity was estimated using a Goldberg optical hand refractometer to measure the total dissolved solids. Concentrations of sulfate and chloride anions, and of calcium, magnesium, sodium, and potassium cations were determined in duplicate using a Dionex-DX100 ion chromatograph. All samples were run at 1:200 dilution. Standards were measured at the start and end of each run to test for drift in the response of the conductivity detector. Precision on separate dilutions was better than 2%. Ammonium, silica, and phosphate concentrations were determined using a Milton Roy Spectronic 301 spectrophotometer. Iron, manganese, lithium, and strontium concentrations were analyzed using a Varian SpectrAA-20 atomic absorption unit. The analytical techniques described by Gieskes et al. (1991) were followed throughout. IAPSO standard seawater was used for calibration.

ORGANIC GEOCHEMISTRY

The following shipboard procedures were followed to measure volatile hydrocarbons, other gases, and high-molecular-weight hydrocarbons, as well as to determine the nature and origin of organic matter in the sediments. These procedures were conducted as part of the routine shipboard safety requirements and to provide preliminary information for shore-based research.

Volatile Hydrocarbons and Other Gases

Low-molecular-weight hydrocarbon samples and other gases were sampled by two different methods. A standard headspace procedure (Kvenvolden and Mcdonald, 1986) involved taking about 5 cm^3 of sediment from each core (axis of freshly cut top of a section) and putting these samples into a 21.5-cm^3 glass serum vial. The vial was sealed with a septum and a metal crimp cap and heated at 60°C for 30 min. A 5-cm^3 volume of gas from the headspace in the vial was extracted with a glass syringe for analysis by gas chromatography.

A vacutainer method of gas collection (Kvenvolden and Mcdonald, 1986) was used where gas pockets or expansion voids were visible in the core, before the core was removed from the plastic liner. A special tool attached to a gas syringe needle and vacutainer was used to penetrate the core liner and collect the gas. Vacutainer gas was routinely analyzed using a Hewlett-Packard 5890 II gas chromatograph (HP), which was modified to measure N$_2$, O$_2$, CO$_2$, and H$_2$S, as well as hydrocarbon gases from methane to hexane. The gas chromatograph

Table 5. Magnetic polarity geochronology of Cande and Kent (1992) used during Leg 150.

Normal polarity interval			Normal polarity interval		
Start (Ma)	End (Ma)	Chron	Start (Ma)	End (Ma)	Chron
0.000	0.780	C1n	22.599	22.760	C6Bn.1n
0.984	1.049	C1r.1n	22.814	23.076	C6Bn.2n
1.757	1.983	C2n	23.357	23.537	C6Cn.1n
2.197	2.229	C2r.1n	23.678	23.800	C6Cn.2n
2.600	3.054	C2An.1n	23.997	24.115	C6Cn.3n
3.127	3.221	C2An.2n	24.722	24.772	C7n.1n
3.325	3.553	C2An.3n	24.826	25.171	C7n.2n
4.033	4.134	C3n.1n	25.482	25.633	C7An
4.265	4.432	C3n.2n	25.807	25.934	C8n.1n
4.611	4.694	C3n.3n	25.974	26.533	C8n.2n
4.812	5.046	C3n.4n	27.004	27.946	C9n
5.705	5.946	C3An.1n	28.255	28.484	C10n.1n
6.078	6.376	C3An.2n	28.550	28.716	C10n.2n
6.744	6.901	C3Bn	29.373	29.633	C11n.1n
6.946	6.981	C3Br.1n	29.737	30.071	C11n.2n
7.153	7.187	C3Br.2n	30.452	30.915	C12n
7.245	7.376	C4n.1n	33.050	33.543	C13n
7.464	7.892	C4n.2n	34.669	34.959	C15n
8.047	8.079	C4r.1n	35.368	35.554	C16n.1n
8.529	8.861	C4An	35.716	36.383	C16n.2n
9.069	9.149	C4Ar.1n	36.665	37.534	C17n.1n
9.428	9.491	C4Ar.2n	37.667	37.915	C17n.2n
9.592	9.735	C5n.1n	37.988	38.183	C17n.3n
9.777	10.834	C5n.2n	38.500	39.639	C18n.1n
10.940	10.989	C5r.1n	39.718	40.221	C18n.2n
11.378	11.434	C5r.2n	41.353	41.617	C19n
11.852	12.000	C5An.1n	42.629	43.868	C20n
12.108	12.333	C5An.2n	46.284	47.861	C21n
12.618	12.649	C5Ar.1n	48.947	49.603	C22n
12.718	12.764	C5Ar.2n	50.646	50.812	C23n.1n
12.941	13.094	C5AAn	50.913	51.609	C23n.2n
13.674	14.059	C5ABn	52.238	52.544	C24n.1n
14.164	14.608	C5ACn	52.641	52.685	C24n.2n
14.800	14.890	C5ADn	52.791	53.250	C24n.3n
15.038	15.162	C5Bn.1n	55.981	56.515	C25n
16.035	16.318	C5Bn.2n	57.800	58.197	C26n
16.352	16.515	C5Cn.1n	61.555	61.951	C27n
16.583	16.755	C5Cn.2n	63.303	64.542	C28n
17.310	17.650	C5Cn.3n	64.911	65.732	C29n
18.317	18.817	C5Dn	66.601	68.625	C30n
19.083	20.162	C5En	68.745	69.683	C31n
20.546	20.752	C6n	71.722	71.943	C32n.1n
21.021	21.343	C6An.1n	72.147	73.288	C32n.2n
21.787	21.877	C6An.2n	73.517	73.584	C32r1n
22.166	22.263	C6AAn	73.781	78.781	C33n
22.471	22.505	C6AAr.1n	83.000	(118.0)	C34n
		C6AAr.2n			

was fitted with thermal conductivity (TCD) and flame ionization (FID) detectors and a series of automatic switching valves that allowed the sequential analysis of C$_1$ to C$_6$ hydrocarbons and provided an automatic backflush. To obtain the separation required, the system used a multicolumn setup composed of a 0.32 cm × 1.8 m stainless steel column—packed with Poropak T (50/80 mesh) Hayset (acid washed)—and a 60 m × 0.32 mm DB-1 capillary column (J & W, Inc.). A Hewlett-Packard 3365 Chemstation computer data collection and analysis system was used to control the automatic valve switching and collect the data. The sample was introduced by means of a 0.5-cm^3 sample loop with automatic backflush. The TCD was kept isothermal at 80°C, while hydrocarbon separation on the FID was performed using a temperature program of 80°–100°C at 8°C/min and then to 200°C at 30°C/min. Helium was used as the carrier gas. The TCD injector and detector temperatures were 80°C and 150°C, respectively, and the corresponding FID temperatures were 150°C and 250°C, respectively. Calibration was made by using Scotty IV analyzed gases, and concentrations were measured in parts per million (ppm).

Gas concentrations and compositions were routinely measured using the Hach-Carle (HC) gas chromatograph. This instrument measures concentrations of methane, ethane, and propane accurately and rapidly. Ethene was resolved from ethane and was quantified. Samples were introduced into the HC gas chromatograph by means of a 1.0-cm^3 sample loop with manual column backflush. The chromatographic column was a 0.32 cm × 1.8 m stainless-steel tubing packed with 80% Poropak N and Poropak Q (80/100 mesh). A flame ionization detector

Table 6. Comparison of Rock-Eval TOC, HI, and OI with TOC derived from the difference method from samples at Hole 904A.

Core, section, interval (cm)	Depth (mbsf)	Rock-Eval			Difference method		
		TOC	HI	OI	TOC	HI	OI
150-904A-							
1H-4, 85–87	5.35	0.37	146	210	0.41	131	190
4H-3, 66–67	31.66	0.40	70	318	0.32	87	396
7H-4, 77–78	61.77	0.43	77	228	0.41	80	239
10H-2, 79–81	87.29	0.32	78	378	0.3	83	403
13H-4, 45–47	115.95	1.25	268	158	1.39	241	141
16H-3, 80–82	143.30	1.66	225	64	1.74	214	60
19H-3, 53–54	171.53	0.49	308	218	0.53	284	201
22H-3, 63–65	200.13	0.80	319	269	1.09	233	197
24H-4, 38–40	217.07	0.44	259	236	0.36	316	288
27X-3, 38–40	245.78	1.57	152	136	1.52	157	140
30X-3, 60–61	274.90	1.41	150	104	1.21	174	120
41X-3, 58–59	378.38	0.28	146	493	0.36	113	383
42X-3, 78–79	388.18	0.25	144	568	0.33	109	430
45X-3, 78–80	417.18	0.42	95	343	0.39	102	369
48X-3, 80–81	445.80	0.16	138	718	0.14	157	821
51X-4, 82–83	476.22	0.28	93	371	0.14	185	742
54X-3, 61–62	503.41	0.17	147	623	0.16	156	662
59X-5, 98–99	544.98	0.17	129	682	0.24	91	483

was used, and the chromatographic conditions were isothermal at 90°C, with helium used as a carrier gas. A Hewlett-Packard 3365 Chemstation computer data collection and analysis system was used to integrate and store the results of the gas measurement.

High-molecular-weight Hydrocarbons

Solvent soluble organic material (bitumen) obtained from 1 to 2 g of sediment from a few carbonate split samples were analyzed by gas chromatography on a Hewlett-Packard Model 5890A gas chromatograph, equipped with a capillary column and split injection. Operating conditions for this instrument were as follows:

1. Column: HP Ultra 1 (Cross-linked Methyl Silicon Gum), 50 m × 0.2 mm × 0.11 m film thickness.
2. Conditions: He = 400 kPa, air = 200 kPa, and H_2 = 150 kPa.
3. Temperatures: injector = 250°C, detector = 300°C, temperature program = initial at 30°C for 3 min, then 10°C/min to 220°C, 4°C/min to 300°C, and held isothermal for 15 min.

Bitumen was analyzed by the method employed during Leg 141 (Behrmann, Lewis, Musgrave, et al., 1992) to obtain indications of the provenance, character, and maturity of the sediment organic matter. To intercalibrate different methods of paleo-sea-surface temperature determinations, measurement of the relative abundances of the long chain di- and tri-unsaturated alkanones was attempted. All glassware was thoroughly washed with tap water and soap, rinsed with nanopure water, dried, and then rerinsed with methanol and dichloromethane (in that order). Each sample was placed in a centrifuge tube. The sample was placed in 10 mL of methanol in an ultrasonic bath for 30 min. Then 5 mL of n-hexane was added and the mixture was shaken for 2 min, followed by centrifugation at 2000 rpm for 5 min. The hexane supernatant was removed by disposable pipette into a 2-mL vial, and the solvent was evaporated to about 50 μL under a stream of He. A 1- to 4-μL sample was injected into the gas chromatograph. Identification of n-alkanes was based on comparison of retention times with those of authentic standards; alkanones and alkanoates, however, were compared with chromatograms in published literature.

Organic Matter Type

The types and quantities of organic matter present in sediment in carbonate split samples taken from each core were evaluated by pyrolysis using the Delsi-Nermag Rock-Eval II system. This system uses a whole-rock pyrolysis technique to identify the type and maturity of organic matter, and to detect the petroleum potential of the sediments (Espitalié et al., 1986). The Rock-Eval system involves a graduated temperature program that first releases volatile hydrocarbons (S_1) at 300°C for 3 min, and then releases hydrocarbons from the thermal cracking of kerogen (S_2) as the temperature increases by 25°C/min from 300° to 600°C. The S_1 and S_2 hydrocarbons were measured by a flame ionization detector and are reported in milligrams per gram of sediment. The temperature at which the kerogen yields the maximum amount of hydrocarbons during the S_2 program provides T_{max}, a parameter that assesses the maturity of the organic matter. Between 300° and 390°C during the pyrolysis program, CO_2 released from the thermal degradation of organic matter (S_3) is trapped and measured by a thermal conductivity detector in milligrams per gram of sediment. The Rock-Eval II instrument is equipped with a TOC facility that calculates the amount of organic carbon in the samples by oxidizing the pyrolyzed sample and using the S_1, S_2, and S_3 values. The Rock-Eval II parameters characterize organic matter by allowing the hydrogen index [(HI); $(100 \times S_2)$/TOC], oxygen index [(OI); $(100 \times S_3)$/TOC], and the S_2/S_3 ratio to be calculated. Interpretations of Rock-Eval are considered to be unreliable for samples containing less than 0.5% TOC (Peters, 1986). A Hewlett-Packard 3365 Chemstation computer-data-analysis system was used to integrate and store the results obtained from the Rock-Eval II instrument. To check the validity of the Rock-Eval-derived parameters (TOC, OI, and HI), the results were compared with the TOC, OI, and HI results obtained by subtracting inorganic carbon obtained from coulometry from total carbon values obtained by combustion and with the S_2 and S_3 values obtained by the combustion method (Table 6).

Fluorescence

The fluorescence of bitumen indicates the aromatic content of the hydrocarbons and therefore provides an approximate measure of the petroleum potential, type, and origin of the sediment organic matter (Curray, Moore, et al., 1982). Fluorescence was determined on total methanol/hexane extracts. These were obtained from 5-cm^3 samples taken from cores where C_1/C_2 and C_1/C_{2+} ratios were particularly low to verify the presence of mature hydrocarbons for pollution-monitoring purposes. The total extract was dissolved in 0.5-mL n-hexane, and fluorescence color and intensity were estimated under an ultraviolet (UV) lamp.

Elemental Analysis

One 5-cm^3 sediment sample taken randomly from each core was analyzed for total carbon (TC), carbonate carbon, total organic carbon (TOC), nitrogen, and sulfur. The carbonate-carbon content of the samples was determined using a Coulometrics 5011 carbonate-carbon analyzer. A sample of about 20 mg of freeze-dried, ground material was reacted with 2M HCl. The liberated CO_2 formed a titratable acid with a blue monoethanolamine indicator solution, which caused the color to fade. The change in color was measured by a photodetector cell that automated a platinum anode to produce base electrically, which in turn returned the indicator to its original color. Carbonate contents are expressed as weight percent $CaCO_3$, assuming all the carbonate was present as calcite.

Total carbon, nitrogen, and sulfur were determined using a Carlo-Erba 1500 CNS Analyzer. About 5 mg of freeze-dried, ground sediment with vanadium pentoxide catalyst added were combusted at 1000°C in a stream of oxygen. Nitrogen oxides were reduced to N_2, and the mixture of SO_2, CO_2, and N_2 was separated by gas chromatography and quantified with a thermal conductivity detector. The total organic carbon of the sediment samples was determined by subtracting the carbonate-carbon from the total-carbon values. The results were compared with the TOC values obtained from the Rock-Eval module (Table 6).

PHYSICAL PROPERTIES

Shipboard measurements of physical properties contribute to characterizing variations in the sediment records caused by environmental changes, depositional and erosional events, and other geological phenomena. They further help to correlate core lithology, downhole geophysical logs, and seismic data.

Wet-bulk density, compressional-wave velocity, magnetic susceptibility, and natural gamma ray emissions were measured in whole-round core sections on the multisensor track (MST). Thermal conductivity measurements using the needle-probe method were performed at discrete intervals in whole-round sections.

Physical properties measurements made in undisturbed sections of split cores included index properties (bulk density, water content, grain density, dry-bulk density, porosity, and void ratio) and compressional-wave velocity. Most samples were extracted at regularly spaced intervals, although some were taken in thin lithologic units that would have been missed by the regular sampling patterns. Sediment induration was measured with a hand-held penetrometer.

Multisensor Track

The multisensor track (MST) incorporated the gamma-ray attenuation porosity evaluator (GRAPE), P-wave logger (PWL), magnetic susceptibility, and natural gamma-ray (MST NGR) devices. All MST measurements are dependent on core diameter and/or volume and therefore are most reliable in APC and undisturbed XCB and RCB cores. XCB and RCB cores often suffer drilling disturbance, have irregular variations in core diameter, and contain voids; corrections must be applied when these data are analyzed. All sections, excluding core catchers and those with deformed core liners, were run through the MST.

The GRAPE determined wet-bulk density at 0.5- to 2-cm intervals by comparing the attenuation of gamma rays through the cores with their attenuation through aluminum standards. Recalibration was required approximately every 24 hr. GRAPE bulk densities were calculated by means of shipboard software using calibration coefficients from the aluminum standard runs. Aluminum has a Compton mass attenuation coefficient of 0.10 cm^2/g, which is also valid for most common minerals. GRAPE bulk densities were not corrected for the presence of water, which has an attenuation coefficient of 0.11 cm^2/g. The so-called "Boyce correction" (Boyce, 1976) for water content can easily be applied to the data as follows:

$$\rho = \rho_s - [(\rho_s' - \rho') \cdot (\rho_s - \rho_{pw})/(\rho_s' - \rho_{pw}')], \qquad (1)$$

where

ρ = GRAPE bulk-density estimate corrected for water content;
ρ' = GRAPE bulk-density estimate uncorrected for water content;
ρ_s = assumed solid matter (grain) density of quartz (2.65 g/cm^3);
ρ_s' = assumed GRAPE estimate of solid matter (grain) density (2.65 g/cm^3)
ρ_{pw} = assumed standard pore-water (seawater) density (1.024 g/cm^3 at salinity = 0.035; Temp. = 20°C);
ρ_{pw}' = GRAPE pore-water density estimate using attenuation coefficient for quartz (1.128 g/cm^3).

The effects of this correction are GRAPE density estimate decreases of 10% for pore water, 0% for quartz, and 3% for a mixture of 50 wt% quartz and 50 wt% pore water (bulk density of 1.8 g/cm^3). Because water contents of more than 50% are rare and measured bulk densities are mostly between 1.8 and 2.2 g/cm^3, the error is generally between 1.5% and 3%. Note that several assumptions must be made for the Boyce correction, which also introduces errors. In particular, all solid matter is assumed to have the density and mass attenuation coefficient of quartz, and pore-water salinity is assumed to be con-

stant. Furthermore, the statistical error of a 2-s GRAPE sample is at least 3% (Boyce, 1976).

The PWL transmits a 500-kHz compressional-wave signal through the cores. Transmitting and receiving transducers are aligned perpendicular to the long axis of the core. A pair of displacement transducers monitors the separation between the compressional wave transducers; variations in the outside diameter of the liner, therefore, do not degrade the accuracy of velocities. Measurements were taken at 2- to 3-cm intervals. Water was sprayed on the outer surface of the core liner to enhance contact between transducers and liner. Poor contact between liner and sediment significantly degraded the data. The receiving transducer in such cases often picked up a spurious signal that gave a uniform apparent velocity of 2100–2200 m/s. The PWL was switched off when results were poor. Aberrant data were discarded.

Magnetic susceptibility was measured on all sections at 10-cm intervals using the 1.0 range on the Bartington Instruments magnetic susceptibility meter (Model MS2) with an 8-cm-diameter loop. Magnetic susceptibility, in addition to assisting with correlation between holes, aids in the detection of fine variations in magnetic intensity associated with magnetic reversals. Magnetic susceptibility results are described in the "Paleomagnetism" section of each site chapter (this volume).

The MST NGR device was used at all sites except Site 902. It provides a means of direct core/log correlation. Its initial use at Sites 903 and 904 was experimental. The period during which gamma rays were counted was initially set at 5 min, and only one measurement was made per core. The counting period was subsequently reduced, and the number of measurements per core increased. In the lower part of Hole 904A and at Site 905, the counting period was set at 30 s and four measurements were made per section. A detailed account of the use of the MST NGR is given in Chapter 5 (this volume).

Thermal Conductivity

Accurate geothermal heat-flow determinations require both thermal conductivity and downhole temperature measurements. Thermal conductivity is the measure of the rate at which heat is transmitted by molecular conduction.

A preprogrammed microprocessor, ThermCon-85, controlled five thermal conductivity probes at a time that heated the tested materials for 6 min and recorded the subsequent temperature responses. The ThermCon-85 microprocessor and a total of 12 probes were calibrated before data acquisition. Calibrations recorded probe drift (rate of temperature change with time) and thermal conductivity measured on three known standards ("black rubber," "red rubber," and "macor"; Table 7). Slope and intercept derived from the needle calibrations were input into the data acquisition program. Conductivities measured in cores were subsequently corrected by means of a least-squares fit to the calibration data. Many control measurements were made during Leg 150 by alternating one of the five probes through a standard material. During periods of rapid core recovery, the standard was sometimes omitted.

Cores were allowed to equilibrate to ambient temperature for a minimum of 4 hr before being analyzed for thermal conductivity. Small holes were drilled through the core liner, and needle probes for full space measurement were inserted. A drift survey was performed until the measured change of temperature with time became ≤ 0.04°C/min. Drift was often allowed to decrease to values ≤ 0.04°C/min. Up to eight measurements per core were made in the intervals in which the ADARA downhole temperature tool was being run. Otherwise, the usual frequency of measurements was three per core.

Data were collected by a microcomputer interfaced directly to the ThermCon-85 box. Temperatures measured between approximately 60 and 240 s from the beginning of the run were fit to the apparent thermal conductivity equation of Von Herzen and Maxwell (1959) by a least-squares regression:

Table 7. Thermal conductivity needle calibration for full space (in W/[m · K]), calibrated and used on Leg 150.

Needle no.:		3	17	150	318	319	320	325	332	338	339	340	341
Black rubber		0.5581	0.5382	0.5487	0.5160	0.5546	0.5395	0.5525	0.5461	0.4847	0.5667	0.5562	0.4733
		0.5542	0.5507	0.5429	0.5644	0.5463	0.5457	0.5873	0.5445	0.4786	0.5676	0.5459	0.4677
		0.5477	0.5534	0.5452	0.5353	0.5435	0.5420	0.5470	0.5435	0.4979	0.5356	0.6211	0.5306
		0.5558	0.5423	0.5498	0.5367	0.5379	0.5407	0.5298	0.5441	0.4854	—	—	0.5109
		0.5488	0.5496	0.5478	0.5300	0.5257	0.5331	0.5465	0.5473	—	—	—	0.5228
	Mean	0.5529	0.5468	0.5469	0.5365	0.5416	0.5402	0.5526	0.5451	0.4867	0.5567	0.5744	0.5011
	SD	0.0045	0.0063	0.0028	0.0176	0.0107	0.0046	0.0212	0.0015	0.0081	0.0182	0.0408	0.0288
Red rubber		1.0249	1.0410	1.0637	1.0635	1.0223	0.9509	1.0380	0.9985	0.9197	1.1642	1.1069	0.7945
		1.0500	1.0409	1.0714	1.0306	1.0483	0.9186	0.9943	1.0086	0.9294	1.2000	1.0010	0.8424
		1.0681	0.9957	1.0551	1.0334	1.0430	0.9506	1.0105	1.0086	0.9293	1.0728	1.0566	0.8284
		1.0646	1.0336	1.0206	1.2072	1.0367	0.9743	0.9952	0.9451	0.9001	—	1.0370	0.8219
		1.0463	1.0486	1.0290	1.0446	1.0262	0.9637	0.9922	0.9942	0.9519	—	1.0993	0.8844
	Mean	1.0508	1.0319	1.0479	1.0759	1.0353	0.9516	1.0061	0.9910	0.9261	1.1457	1.0602	0.8343
	SD	0.0172	0.0210	0.0221	0.0746	0.0110	0.0209	0.0193	0.0264	0.0187	0.0656	0.0441	0.0330
Macor		1.9703	1.9090	1.9531	1.9229	1.7866	1.8984	1.6981	1.8569	1.5261	2.0735	1.6826	1.7782
		1.9951	1.8350	1.8347	1.8988	1.9850	1.8820	1.7653	1.8908	1.4661	1.8004	1.9535	1.7725
		1.8351	1.7299	1.9024	1.6382	1.8730	1.8732	1.9558	1.8777	1.2888	2.0010	1.8983	1.7713
		1.8384	1.7547	2.0706	1.8762	1.8320	1.8822	1.6364	1.8641	1.4755	—	2.0919	1.6189
		2.0466	1.8763	1.8804	1.9168	1.8622	1.9186	1.6799	1.8479	1.5376	—	1.9970	1.5765
	Mean	1.9371	1.8210	1.9282	1.8506	1.8678	1.8909	1.7471	1.8675	1.4588	1.9583	1.9246	1.7035
	SD	0.0957	0.0770	0.0903	0.1201	0.0736	0.0180	0.1255	0.0170	0.1000	0.1415	0.1528	0.0977
Summary	Known	Mean	Mean	Mean	Mean	Mean	Mean	Mean	Mean	Mean	Mean	Mean	Mean
Black rubber	0.54	0.5529	0.5468	0.5469	0.5365	0.5416	0.5402	0.5526	0.5451	0.4867	0.5567	0.5744	0.5011
Red rubber	0.96	1.0508	1.0320	1.0479	1.0759	1.0353	0.9516	1.0061	0.9910	0.9261	1.1457	1.0602	0.8343
Macor	1.61	1.9371	1.8210	1.9282	1.8506	1.8678	1.8909	1.7471	1.8675	1.4588	1.9583	1.9247	1.7035
Linear regression	Slope	0.7684	0.8382	0.7705	0.8160	0.8041	0.7749	0.8940	0.7998	1.1048	0.7656	0.7877	0.8613
	Intercept	0.1298	0.0867	0.1319	0.0948	0.1134	0.1629	0.0516	0.1293	-0.0209	0.1025	0.1021	0.1642

Note: SD = standard deviation. Dash (—) = no measurement.

$$T(t) = (q/4\pi k) \times \ln(t) + L(t), \qquad (2)$$

where

k = apparent thermal conductivity (W/[m · K]),
T = temperature (K),
t = time (s),
q = heat input per unit length of wire per unit time (W/[m · s]), and
L = a correction factor for temperature drift that is described by

$$L(t) = At + T_e, \qquad (3)$$

where

A = rate of temperature change and
T_e = equilibrium temperature.

The regression yields k, thermal conductivity, and A, rate of temperature change. Errors are between 5% and 10%. Corrections were not attempted for in situ temperature or pressure effects. Measurements accompanied during processing by "high drift" or "high error" messages were discarded before plotting the results.

Index Properties

Index properties (bulk density, water content, grain density, dry-bulk density, porosity, and void ratio) were calculated from measurements of wet and dry sample masses and volumes (MV method) of discrete sediment samples of approximately 10 cm³.

Samples were placed in premeasured aluminum containers (beakers) before measuring mass and volume. Sample mass was determined to a precision of ±0.05 g using a Scientech electronic balance. Wet sample volumes were determined using a Quantachrome Penta-Pycnometer, a helium-displacement pycnometer with five sample cells. A reference volume was run with each group of samples, except during short periods of high sample turnover, and rotated among the cells to check for error. Ideally, a precision of ±0.02 cm³ should be

maintained when measuring the volume of the 16.38-cm³ reference. Pycnometer cell volumes were recalibrated frequently when the error was found to exceed 0.02 cm³. This did not always improve the precision; errors, therefore, were probably sometimes greater than the optimum value. The precision of measuring the reference volume could vary from –0.05 to +0.02 cm³ (measured reference volumes differing by more than 0.02 cm³ from the nominal value were invariably less than the nominal reference volumes). For each set of samples, the pycnometer was first run with a helium purge of 3 min, followed by two successive purges of 1 min each. Sample volume was determined by averaging the volumes resulting from the last two (1 min) runs. Dry mass was measured for samples that had been oven dried at 110° ± 5°C for 24 hr and cooled in a desiccator for 2 hr. Dry volumes of at least one sample per core were measured after dry mass determination at Sites 903, 904, and 905. This practice was adopted because grain densities calculated from wet volumes at Site 902 proved to be unrealistically high (generally 2.7–3.0 g/cm³).

Bulk density, water content (wet and dry), grain density, porosity and void ratio computations were made automatically within the index properties data program IP/4D, used for the first time on Leg 150. Calculated values include correction for salt, assuming a standard pore-water salinity of 0.035 (pore-water density of 1.024 g/cm³).

Compressional-wave Velocity

Velocity calculations used measurements of traveltime for a compressional-wave signal sent between two transducers through a sediment sample of known length. Most velocity measurements were oriented parallel to the core axis, but some measurements were made perpendicular to the core axis.

Two instruments were used. A Dalhousie University/Bedford Institute of Oceanography Digital Sound Velocimeter (DSV; see Leg 138 "Explanatory Notes" chapter in Mayer, Pisias, Janacek, et al., 1992) was used for measuring sound velocity along the core axis (i.e., vertically) in soft sediment. The two DSV transducers were mounted with a fixed separation and emitted a 2-μs square wave signal at a frequency of 60 Hz. The signals transmitted and received by the DSV

were digitized by a Nicolet 320 digital oscilloscope and transferred to a microcomputer for processing. The transducers were inserted into sediment in split cores. The DSV tool was periodically calibrated in distilled water.

The Hamilton Frame velocimeter was used when the sediment became too hard to insert the DSV transducers. A Tektronix DC 5010 counter/timer system emitted and received a 500-kHz signal through two transducers of adjustable separation. The Hamilton Frame was periodically calibrated with lucite standards to a precision of 1%. Lithified samples were cut into blocks with at least one pair of parallel sides (usually perpendicular to the core axis). Acoustic contact between transducers and sample was improved by adding small amounts of distilled water at the contacts. Some attempts, usually unsuccessful, were made to measure compressional-wave velocities of sediment in split liners. Sample thickness was measured using a mechanical analog gauge attached to the Hamilton Frame. The precision of thickness measurements was ±0.1 mm. Overcoming the effects of high signal attenuation required reduction of sample thicknesses to 10 mm or less. Repeated Hamilton Frame measurements on single samples indicated a precision of ±30 m/s.

For both instruments, computer software summed the waveforms from three successive digital records and displayed the resultant waveform on the oscilloscope. A first-break traveltime was picked automatically using a threshold of approximately 1.04 μV. Traveltime was corrected for hardware delays. Sediment temperatures were measured using a digital thermometer probe and entered as a correction factor in the calculation of compressional velocity.

Velocity measurements at Sites 902, 903, and 905 were adversely affected by fracturing within cores, possibly associated with observed gas expansion. Results improved at Site 904, where sediment was more coherent and degassing was not observed.

Penetrometer

A Soil Test CL-700, hand-held penetrometer was used to estimate sediment induration. Two measurements per section were made at Site 902. At subsequent sites, the number of measurements was reduced to three per core. Penetrometers are designed for use in soft sediment and readings were discarded if the sediment cracked during measurement. If the reading exceeded the maximum range of the instrument (4.5×10^5 Pa), or if no penetration was achieved, a reading of 5×10^5 Pa, the maximum measurable, was assumed for graphical display.

APC DOWNHOLE TEMPERATURE MEASUREMENTS

The APC downhole temperature (ADARA) tool was deployed at Sites 902 and 903. The objective was to investigate the sedimentary record of Holocene changes in bottom-water temperature that may reflect climatic changes. The tool was used to a maximum total depth of 150 m at the highest possible resolution of one per APC core, or every 9.5 m if full APC strokes were achieved.

The tool was built by the geotechnical company Adara for ODP; it consists of a single resistance temperature device, a microprocessor for storing recorded temperatures, and a self-contained power supply. It fits within an annular cavity of a modified APC coring shoe and is capable of temperature measurements with at least 0.01°C precision. Four of the tools were deployed on Leg 139, and all 10 tools have been available since Leg 146. Detailed descriptions of data acquisition and processing are given in the "Explanatory Notes" chapter of the Leg 139 *Initial Reports* volume in Fisher and Becker (1993) and in Horai and Von Herzen (1985).

APC temperature measurements can generally be made beginning with the third APC core, when the bottom-hole assembly is sufficiently buried to allow safe deployment. During Leg 150, temperatures were measured at the mud line (usually before APC release,

sometimes after sub-bottom measurement, occasionally both) and at maximum penetration of each APC over a 10-min interval sampled every 5 s. Shore-based calibration in early 1993 (A. Fisher, unpubl. data) suggested that the electronically most stable probes are 12, 13, and 18. Tools 17 and 16 are less stable. The remaining tools (10, 11, 14, 15, and 19) have not yet been subject to this additional calibration. This extra ("hyper") calibration was accomplished in a large, well-mixed water bath at 5°C increments over a range of standards traceable to the National Institute of Standards and Technology.

Post-cruise temperature estimates using corrections based on shore-based calibrations are reported in this volume. Several factors may result in revised temperature estimates in the future. Selecting a suitable data interval for calculation of the equilibrium temperature is a somewhat subjective process although it can be made consistent by comparing the results of processing different data intervals. Depths of measurements and irregularities in some temperature decay curves need further investigation. In addition, the use of the correct thermal conductivity is required to obtain accurate results. A more rigorous core-hole correlation is therefore needed.

The depth of an APC temperature measurement is assumed to be the bottom of the cored interval. The error in this assumption always is at least ±0.2 m. Greater errors can occur if there is an incomplete stroke of the APC barrel. Nonetheless, the depth scale for thermal conductivity measurements as reported in this volume is uncorrected.

Full APC stroke is assumed if (1) the pressure decrease after failure of the shear pin is instantaneous, (2) the recovered material has a length between 100% and 110% of the core barrel (~10 m), and (3) the recovered material does not show flow-in structure. The speed of the pressure decrease cannot easily be quantified and requires good communication with the driller and/or experience in observing the pressure gauge. If the pressure "bleeds out" slowly and the core barrel is less than 100% full, the stroke is assumed to be incomplete. In this case, the temperature probe will not have measured at $z + 9.5$ m depth, even if the Operations Superintendent decides to advance the bit and continue APC coring at that depth. Flow-in structures are relatively easy to recognize and are likely to indicate incomplete penetration, which allows flow-in of hole-wall material during withdrawal of the core barrel (the "syringe effect"). If pressure decrease shows no unusual pattern, no flow-in is observed, but substantially <10 m of core is recovered, material may have been lost by gravity or gas pressure expulsion between the time the APC was shot and the time the core was dissected on the catwalk.

Thermal conductivity measurements, used to calculate equilibrium temperatures from the temperature decay curve, are made relative to the curatorial depth scale. This scale is expanded in a nonlinear fashion relative to the coring scale as a result of elastic rebound, gas expansion, and drilling disturbances within the retrieved core. All these factors shift the lowermost shipboard thermal conductivity measurements, which are closest to the depth of the Adara measurements, to depths that are beneath the temperature probe. Preliminary estimates suggest that elastic rebound and gas voids encountered on Leg 150 can shift the bottom of full-recovery cores by 0.5 to 2 m within the interval of methane-rich sediment between depths of 30 to 140 mbsf.

For initial processing of Leg 150 APC temperature data, thermal conductivity measurements were averaged using a 4-m box car (2 m on each side of the assumed APC temperature station) to derive a value to be used with the analysis program. This averaging interval introduces some systematic error based on the estimates above and smooths potentially significant variations, considering that several changes of 0.6 W/(m · K) (100% of total variability) occur over 2 m at Site 902. Careful core-to-hole correlation will allow more accurate location of the thermal conductivity measurements relative to the temperature stations, and, thus, more accurate temperature estimates may be provided in the future.

For an assumed thermal conductivity, temperature errors were estimated by comparing final temperature values derived by process-
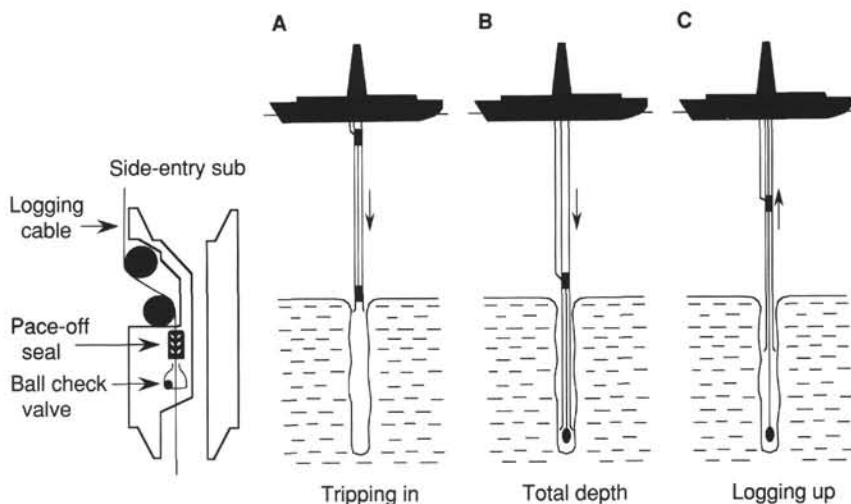
Figure 8. Logging using the side-entry sub. **A.** Logging string inside the drill pipe during descent to seafloor. **B.** Drill pipe and tool string together to total depth. **C.** The drill pipes are moving up ahead of tool string. (From ODP Logging Manual, LDEO, 1990.)

Table 8. Sampling interval, vertical resolution, and measuring points.

Tool string	Tool	Sampling interval	Vertical resolution (m)	Measuring point (m)
Quad-combo tool	NGT	0.5 ft/15 cm	0.2–0.31	30.61
	LSS/SDT	0.5 ft/15 cm		
	CNTG		0.6	
	HLDT	0.5 ft/15 cm	0.3	
	CALI			10.31
	DIT (deep)	0.5 ft/15 cm	¯2	2.90
	DIT (medium)	0.5 ft/15 cm	¯1.5	1.83
	SFL	0.5 ft/15 cm	¯1	1.98
Geochemical	NGT	0.5 ft/15 cm	0.2–0.31	16.87
	CNTG	0.5 ft/15 cm	0.25	
	AACT			10.57
	GST		0.2–0.31	2.84
Formation MicroScanner	NGT	0.5 ft/15 cm	0.2–0.31	9.83
	CALI	1.5 in./3.8 cm		0.33
	GPIT	1.5 in./3.8 cm		0.33
	FMS/SHDT	0.1 in./2.5 m	0.003	0.33

Note: The measuring points above are valid when no LDEO temperature tool (TLT) is attached; otherwise, 1.52 must be added to each value.

ing different sections of the temperature curves. No error is less than about ±0.1°C; more work on data selection for temperature calculation may possibly reduce the error to ±0.05°C in some cases.

DOWNHOLE LOGGING

Downhole wireline-log measurements are made to describe the structure as well as the geochemical and geophysical properties of formations penetrated by the borehole. Downhole measurements in open holes have two advantages over core measurements taken in a laboratory: (1) they measure parameters in a stress and temperature environment that is more representative of in situ conditions than are measurements performed in the laboratory, and (2) they can provide measurements from zones with poor core recovery.

During Leg 150, four different tool strings attached to a seven-conductor cable were used. Logging began after coring was completed and the borehole was flushed of debris and mud. The bottom of the drill pipe was positioned approximately 90 mbsf, and the logging tools were lowered into the borehole through the drill pipe. When poor hole conditions were either known or anticipated, the side-entry sub (SES) was used (see Fig. 8). The SES allows the tool to remain in the hole while pipes are added or removed, and allows water to be pumped down the drill string; it does not permit drill-string rotation. Nonetheless, the SES makes logging possible despite poor hole conditions by allowing the logging tool to follow the pipe up the hole, thereby providing the tool a clear path. A wireline heave

compensator was used at several sites to minimize tool motion during rough weather.

Logging depths are measured relative to the seafloor determined by drilling. Because the sensors are located at various distances from the bottom of the tool string (see Fig. 9), the lowermost parts of the boreholes cannot be completely logged. The tool sampling interval and vertical resolution as well as the measuring points (counted from the bottom of the tool string) are presented in Table 8.

Tool Combinations

On Leg 150 the following four Schlumberger tool strings were used: (1) sonic-induction, (2) porosity, (3) geochemical, and (4) Formation MicroScanner (FMS) (Fig. 9). In addition, a temperature tool (TLT) from Lamont-Doherty Earth Observatory was attached to the bottom of the Schlumberger strings. The sonic-induction tool string consists of the digital sonic, natural spectral gamma-ray, dual-induction resistivity, and mechanical caliper devices. The porosity tool string includes the natural spectral gamma-ray, neutron porosity, and litho-density (with caliper) tools. The geochemical string consists of the natural spectral gamma-ray, aluminum activation clay, and induced gamma-ray spectroscopy tools. Finally, the FMS is run together with a general purpose inclinometer and natural spectral gamma-ray tool. The sonic-induction and porosity tool strings were combined as one geophysical tool string (the Quad combo) for one run at Hole 903C; they were normally run separately to optimize the readings from the sonic and lithodensity tools. The sonic needs to be centralized in the borehole to get good readings; the lithodensity tool, on the other hand, needs to be pressed against the borehole wall. One exception occurred in Hole 903C, in which the Quad combo was used to gain time under deteriorating hole conditions.

Logging Tools

The following is a short description of the different logging tools used during Leg 150. A more complete description can be found in standard reference books (e.g., Schlumberger, 1989, and Serra, 1984, 1989).

Mechanical Caliper Device

The mechanical caliper device (MCD) measures the diameter of the borehole. The borehole diameter is one of the factors that significantly affects many of the other logging measurements and is an important input when other logs are corrected. The caliper device is subject to sticking when formation mud gets into the mechanical parts, which can result in erroneous readings. In contrast, the high-temperature litho-density tool uses a bowspring to press the tool against the borehole
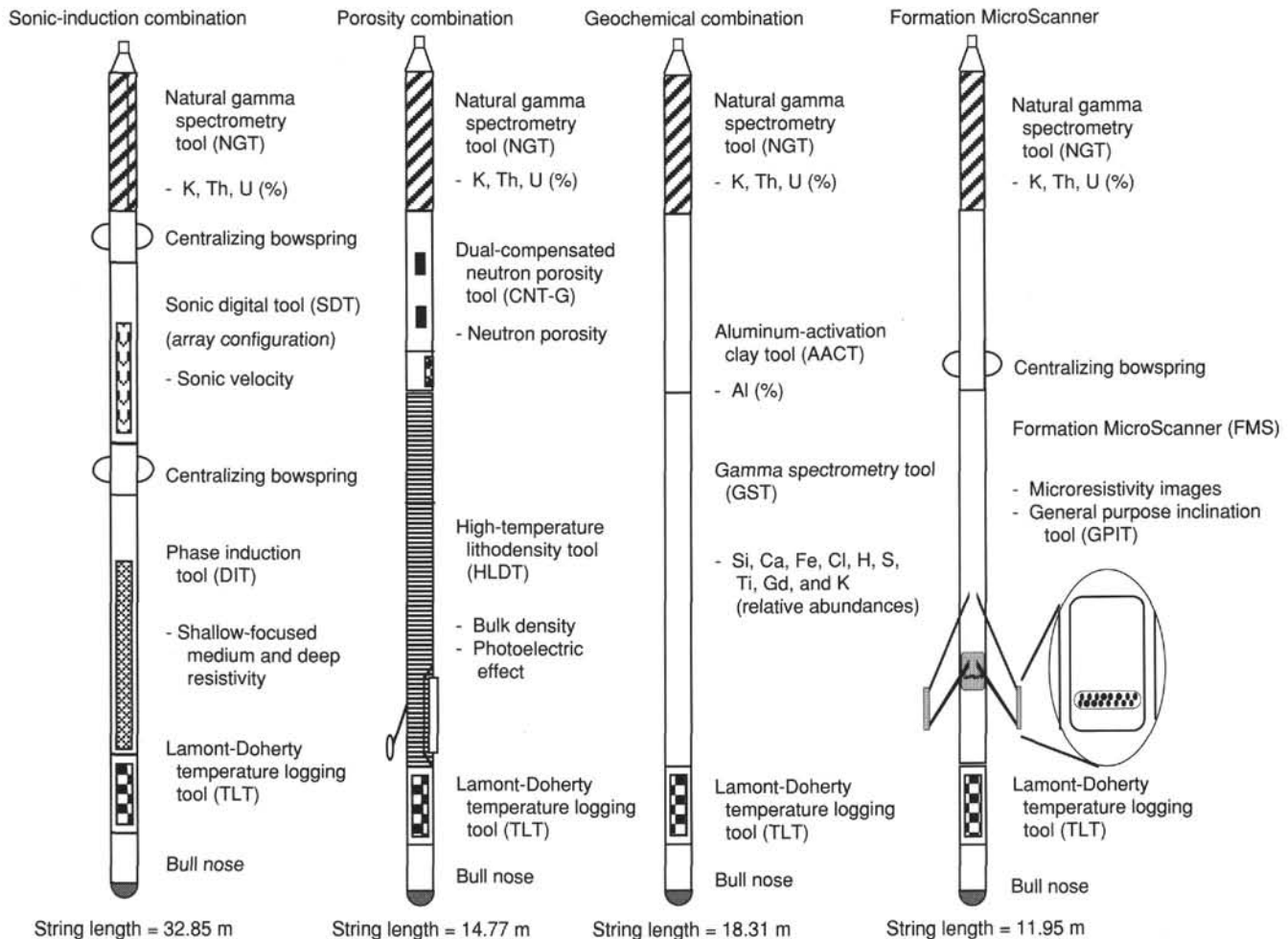
Figure 9. The four log strings used on Leg 150.

wall, which yields a more reliable diameter reading. Consequently, on Leg 150 the caliper device was used more as a centralizer for the sonic tool than as an instrument for measuring the hole diameter.

Natural Gamma Spectrometer

The natural gamma spectrometry (NGT) device measures the natural gamma radiation from the formation. Most gamma rays are emitted from the radioactive isotope ^{40}K and from the U and Th series. The gamma radiation from the formation is measured by a sodium iodide-activated scintillation crystal mounted inside the probe. The gamma rays are analyzed by subdividing the gamma-ray spectrum into five discrete energy windows. The total counts recorded in each window are processed to give estimates of total abundances of K, U, and Th.

Because radioactive elements tend to be more abundant in clay minerals, the gamma-ray curve is often used for determining clay and shale content. The average depth of investigation into a sedimentary formation for the NGT is about 0.3 m. This tool is run in every tool string to enable depth and cross correlation between the different logs.

Lithodensity Tool

A ^{137}Ce gamma-ray source is used in the lithodensity (HLDT) tool, which measures the resulting flux at fixed distances from the source. Normally, the attenuation of gamma rays is caused by Compton scattering (Dewan, 1983). If one assumes that the atomic weight of most rock-forming elements is approximately twice their atomic number,

then the formation density can be extrapolated from the energy flux. A photoelectric effect index is also provided by these measurements. Photoelectric absorption occurs in the energy window below 150 keV, and it is dependent on the energy of the incident gamma ray, the atomic cross section, and the type of atom. This measurement is almost independent of porosity and can be used, therefore, as an indicator of matrix lithology. The tool is pressed against the borehole wall by a strong bowspring arm. If roughness is present in excess of the bowspring capacity, drilling fluid between the tool and formation will cause density readings that are artificially low.

Dual-induction Tool

The dual-induction tool (DIT) measures the electrical resistivity of the borehole surroundings with three different sensing radii. The first two measurements are the "deep" and "medium" resistivities, and they follow the same principle. An alternating high-frequency current is sent through the transmitter coils in the tool body. This creates a magnetic field that induces a secondary current in the formation. The current created in this way generates a new inductive signal that is proportional to the conductivity of the formation. This signal is registered by receiving coils in the tool and is converted thereafter to resistivity values. The third resistivity measurement is made by measuring the current necessary to maintain a constant voltage drop across a fixed interval. This is called "spherically focused resistivity."

Resistivity is a function of the inverse square root of porosity (Archie, 1942). Other factors can influence resistivity, however (e.g.,

temperature, fluid salinity, hydrocarbon content, and clay content). The vertical resolution is about 1 m for the spherically focused resistivity and approximately 2 m for the other two resistivities.

Long-spaced Sonic Tool and Sonic Digital Tool

Both the long-spaced sonic (LSS) and the sonic digital (SDT) tools measure the compressional-wave velocity of the formation. The LSS tool is the basic sonic tool, and it is configured with two acoustic sources 2 ft apart and two receivers also spaced 2 ft apart. The spacing between the receiver pair and the transmitter pair is 8 ft. The tool measures traveltime in microseconds over a certain distance in the formation. The configuration of the tool allows eight different traveltime measurements. The velocity data together with the formation density can be used to generate a synthetic seismogram.

The SDT is a digital version of the basic sonic tool. To the tool is added an 8-array receiver section that enables recordings of many more sonic waveforms at a given depth. The increased amount of data allows more advanced seismic signal processing that will enhance data quality. This tool greatly improves shear and Stoneley wave detection.

Formation MicroScanner

The function of the Formation MicroScanner (FMS) tool is almost the same as that of the dipmeter tool. A general purpose inclinometer (GPI) is included in the string for registration of the position and orientation of the tool. The GPI instrument provides magnetometer and accelerometer data. The FMS uses four orthogonal pads that are pressed against the wall of the borehole during the measurements. On each pad are 16 electrode buttons spaced about 2.5 mm apart and located in 2 (diagonally offset) rows, 8 in each. A focused current is transmitted by the electrodes, and the measurements are presented as a series of curves that show variations in microresistivity of the formation.

When the microresistivity values are processed, the log provides an image of the borehole wall that resembles core photos. The FMS tool makes it possible to detect very thin fractures and detailed sedimentological or structural features. The instrument can detect fractures that range from millimeters to several centimeters across.

The FMS can also be used for imaging the directions of breakouts, which are used to analyze the in-situ stress field around the borehole. Breakouts form in the direction of the least principal horizontal stress in an isotropic, linearly elastic rock subjected to an anisotropic stress field. Bell and Gough (1979) and Zoback et al. (1987) have demonstrated that the stress orientations inferred from rock breakouts are consistent with other independent stress indicators.

Dual-compensated Neutron Porosity Tool

The dual-compensated neutron porosity (CNT-G) tool emits high-energy neutrons (4 MeV) into the formation, where they are scattered and slowed down by collisions with other nuclei. At an energy level of 0.025 MeV, the neutrons are captured and absorbed by atomic nuclei such as hydrogen, silicon, boron, and chlorine. Because the scattering cross-section for hydrogen is approximately 100 times larger than that for any other common element, most of the energy dissipation is caused by collision with water molecules. Hence, the number of neutrons registered by a detector can be related to the water content in the formation. In practice, an array of detectors is used to minimize the hole size and drilling fluid effects. Because water is present both in pores and as bound water (e.g., clay minerals), the true porosity is often overestimated when measured in the presence of hydrous minerals.

Aluminum Activation Clay Tool

The aluminum clay tool (AACT) is essentially a modified NGT tool. To increase the detailed analysis of the spectrum, more windows have been added to the tool. Aluminum abundance is determined by neutron-induced, gamma-ray spectrometry. The source used in the tool is californium. The decay of nuclei generates gamma rays that can be detected within a series of energy windows. To correct for the natural gamma radiation, detectors are placed on both sides of the source to measure natural gamma radiation.

Calibration to elemental weight is accomplished by taking cores of known composition, volume, and density that have not been radiated and measuring their gamma-ray output. This is normally done after logging, in a jig attached to the logging tool.

Gamma-ray Spectrometry Tool

The gamma-ray spectrometry tool (GST) consists of a pulsed source of 14 MeV and a gamma-ray scintillating detector. Shore-based interpretation of this log has to be made so as to describe the actual element abundances. Aboard the ship, a computer is used to perform spectral analysis of the gamma rays generated by the interactions between the emitted neutrons and the atomic nuclei in the formation. Gamma rays from the six elements calcium, iron, silicon, hydrogen, chlorine, and sulfur dominate the spectrum and provide estimates of their abundances.

Lamont-Doherty Temperature Logging Tool

The Borehole Research Group at LDEO has designed a self-contained temperature tool (the TLT) that can be attached to the bottom of the Schlumberger tool strings. Temperature measurements are made by two thermistors: a fast-response thermistor that will detect any short temperature change, and a high-precision one that is more stable and accurate. The tool also includes a pressure transducer that allows the operator to trigger the recording at preprogrammed depths. Inside the tool, a data logger records the readings of the two thermistors and of the pressure transducer every second, and stores them in its memory for up to 9 hr. When the tool is back on deck, the data are downloaded into a Macintosh computer for further processing, starting with merging with the depth recorded by the Schlumberger logging unit.

Log Data Quality

Log data can be degraded in various ways, and their quality differs between tools. Borehole diameter and the shape of the borehole wall are two basic parameters affecting the quality of measurements. Velocity and resistivity logs are less affected by the borehole shape than are neutron porosity, density, and gamma logs, which are very sensitive to the borehole geometry because of the large attenuation of neutrons by the borehole fluid. Corrections for the geometry, however, can be made to the original data to improve log quality.

Logs from different tool strings can have minor depth mismatches, which are caused by either ship heave or cable stretch during measurements. Even small errors in depth match can seriously impair the results in zones with rapidly varying lithology. To minimize the effect of ship heave, a hydraulic heave compensator is used to adjust for rig motion during logging.

Most of the log measurements are performed a short time after completion of the drilling and wiper trips, and consequently the temperature tool can record temperatures very different from the actual formation equilibrium temperature profile. Based on the time elapsed after drilling and the fluid circulation history, these logs can be corrected during shore-based processing, following the methods of Bullard (1947) and Shen and Beck (1986).

Log Analysis

Shipboard Log Processing

During the actual logging operation, data from the tools are recorded on digital disks and displayed in real time on a color monitor

in the Schlumberger logging unit. Starting with Leg 149, Schlumberger uses a new MAXIS 500 digital logging unit in conjunction with the offshore service unit (OSU). The Maxis 500 system generates data in DLIS format (Digital Log Information Standard). During Leg 150, data were converted to LIS format (Log Information Standard) for compatibility with on-board and shore-based logging software. After completion of the logging run, the digital data are transferred to a SUN Computer system in the Downhole Measurement Lab. Here, the field data are reformatted to ASCII format for use in various graphic programs and are made available to the Shipboard Scientific Party. The FMS data are partially processed on board with Schlumberger 'Logos' software. Preliminary log interpretations were conducted aboard ship. Final depth shifting and data quality control were undertaken after the cruise at the Borehole Research Group of LDEO. Further FMS and geochemical processing were conducted at Institute Mediterranéan de Technologie, Technopol de Chateau Gombert in Marseille, France, and at the Borehole Research Department of Geology, University of Leicester, respectively. The FMS data were partially processed on board with Schlumberger 'Logos' software. Preliminary log interpretations based on plots shown within each site chapter were conducted aboard ship.

Shore-based Log Processing

Additional log processing and display were performed post-cruise at each of the three sites of the Borehole Research Group (BRG), using Schlumberger "Logos" software and additional programs developed by members of the BRG. Displays of most of these processed data appear with accompanying text at the end of the appropriate site chapters in this volume. Files of all processed logs (including FMS, dipmeter, and BRG temperature data not shown in printed form) plus explanatory texts are included on the CD/ROM disk enclosed in the back pocket of this volume; a directory of the contents of the disk is found at the front of this volume.

Shore-based processing of data from each hole consisted of (1) depth adjustments of all logs to a common measurement below the seafloor, (2) corrections specific to certain tools, and (3) quality control and rejection of unrealistic values.

The depth-shifting procedure is based on an interactive, graphical depth-match program that allows the processor to visually correlate logs and define appropriate shifts. The reference log and the log to be adjusted in depth are displayed side-by-side on a screen, and vectors connect the two at positions chosen by the user. The total gamma-ray curve (SGR) from the NGT tool run on each logging string was used in most cases to correlate the logging runs. In general, the reference curve is chosen on the basis of constant, low cable tension and high cable speed (tools run at faster speeds are less likely to stick and are less susceptible to data degradation caused by ship heave). Other factors, however, such as the length of the logged interval, the presence of drill pipe, and the statistical quality of the collected data (better statistics are obtained at lower logging speeds) are also considered in the selection. A list of the amount of differential depth shifts applied at each hole is available upon request to BRG (LDEO) and in the "dshift.doc" file on the enclosed CD-ROM disk.

Specific tool corrections were performed on the gamma-ray data to account for changes in borehole size and for the composition of the drilling fluid. Processing techniques unique to the ACT and GST tools of the geochemical string are described in detail below.

Quality control was performed by cross-correlation of all logging data. If the data processor concluded that individual log measurements represented unrealistic values, the choices were either to discard the data outright and substitute the null value of "–999.25" or to identify a specific depth interval containing suspect values that must be used with caution. The latter are noted in the text that accompanies all processed log displays. Quality control of the SDT acoustic data was based on discarding any of the four independent transit time measurements that were negative or that fell outside a range of reasonable values selected by the processor.

Locally, some intervals of log data appeared unreliable (usually due to poor hole conditions) and were not processed beyond what had been done on board the ship. In general, a large (>12 in.) and/or irregular borehole affects most recordings, particularly those that require eccentralization (CNTG, HLDT) and a good contact with the borehole wall. Hole deviation can also degrade the data; the FMS, for example, is not designed to be run in holes that are more than 10° off vertical, as the tool weight might cause the caliper to close.

For further information on the wireline logs, contact Cristina Broglia or Elizabeth Pratson, Borehole Research Group, Lamont-Doherty Earth Observatory, Palisades, NY 10964, U.S.A. (phone: 914-365-8313; fax: 914-365-3182; email address: beth@Ideo.columbia.edu).

Shore-based Geochemical Log Processing[3]

The geochemical logging tool string (GLT) run at Site 906 included the natural gamma-ray spectrometry tool (NGT), the compensated neutron tool (CNT), the aluminum activation clay tool (AACT), and the gamma-ray spectrometry tool (GST). Results are discussed in the "Downhole Logging" section of Chapter 10 (this volume) and displayed in Figure 22 (same chapter). The following describes the various tools within the GLT and how the data have been processed.

The NGT, CNT, and AACT use three separate modes of gamma-ray spectroscopy for a comprehensive elemental analysis of the formation. The NGT, located at the top of the tool string, measures the naturally occurring radionuclides, thorium (Th), uranium (U), and potassium (K), before the formation is irradiated by the nuclear sources contained in the lower tools (Fig. 9). The CNT, located below the NGT, carries a californium (^{252}Cf) neutron source to activate the Al atoms in the formation. The AACT, a modified NGT, is used to measure the activated gamma rays in the formation. By combining the AACT measurement with the previous NGT measurement, the background radiation is subtracted out and a reading of formation Al is obtained (Scott and Smith, 1973). The gamma-ray spectrometry tool at the base of the string carries a pulsed neutron generator to induce prompt-capture gamma-ray reactions in the borehole and formation and a NaI(Tl) scintillation detector to measure the energy spectrum of gamma rays generated by the prompt neutron capture reactions. As each of the elements in the formation is characterized by a unique spectral signature, it is possible to derive the contribution (or yield) of each of the major elements silicon (Si), iron (Fe), calcium (Ca), titanium (Ti), sulfur (S), gadolinium (Gd), and potassium (K) from the measured spectrum and, in turn, to estimate the relative abundance of each in the formation when combined with the elemental concentrations from the NGT and AACT. The GST also measures the hydrogen (H) and chlorine (Cl) in the borehole and formation, although these elements are not used for determining the rock geochemistry.

The only major rock-forming elements not measured by the geochemical tool string are magnesium (Mg) and sodium (Na); the neutron-capture cross sections of these elements are too small relative to their typical abundances for the GLT to detect. A rough estimate of Mg + Na can be made in some instances by using the photoelectric factor (PEF), measured by the lithodensity tool (Hertzog et al., 1989). This calculation was not implemented on the geochemical data from Hole 906A as the (Mg + Na) component was below the detection resolution of this technique.

Processing of the spectrometry data was required to transform the relative elemental yields into oxide weight fractions. It was performed with a set of log-interpretation programs written by Schlumberger that have been slightly modified to account for the lithologies

---

and hole conditions encountered in ODP holes. The processing steps are summarized below.

Step 1: Reconstruction of Relative Elemental Yields from Recorded Spectral Data

This first processing step compares the measured spectra from the gamma-ray spectrometry tool with a series of "standard" spectra to determine the relative contribution (or yield) of each element. These "standards" approximate the spectrum of each element. Using a weighted, least-squares inversion method, the relative elemental yields are calculated at each depth level.

Six elemental standards (Si, Fe, Ca, S, Cl, and H) are used to produce the shipboard yields, but three additional standards (Ti, Gd, and K) can be included in the post-cruise processing to improve the fit of the spectral standards to the measured spectra (Grau and Schweitzer, 1989). Although Ti, Gd, and K often appear in the formation in very low concentrations, they can make a large contribution to the measured spectra because they have large neutron-capture cross sections. For example, the capture cross section of Gd is 49,000 barns, whereas that of Si is 0.16 barns (Hertzog et al., 1989). Therefore, including Gd is necessary when calculating the best fit of the standard spectra to the measured spectrum.

The elemental standards (Si, Ca, Fe, Ti, Gd, K, Cl, and H) were used in the spectral analysis step for Hole 906A. The spectral standard for S was not used because this element exists in concentrations generally below the detection resolution of the tool in this hole; the inclusion of S in the spectral inversion was found to increase the noise level significantly in the other elemental yields. A linear seven-point (3.5 ft, 1.067 m) moving average was applied to the output yields to increase the signal-to-noise ratios.

Step 2: Depth Shifting

Geochemical processing involves the integration of data from the different tool strings; consequently, it is important that all the data are depth correlated to one reference logging run. The NGT, run on each of the logging tool strings, provides a spectral gamma-ray curve with which to correlate each of the logging runs. A reference run was chosen on the basis of constant and low cable tension as well as high cable speed (tools run at faster speeds are less likely to stick and are less susceptible to data degradation caused by ship heave). The depth-shifting procedure involves picking a number of reference points based on similar log character and then invoking a program that expands and compresses the matching logging run to fit the reference logging run. The lithodensity tool string was chosen as the reference run in Hole 906A.

Step 3: Calculation of Total Radioactivity and Th, U, and K Concentrations

The third processing routine calculates the total natural gamma-ray radiation in the formation in addition to concentrations of Th, U, and K, using the counts in five spectral windows from the NGT (Lock and Hoyer, 1971). This routine resembles shipboard processing; however, results were improved during post-cruise processing by including corrections for hole-size changes and temperature variations. Kalman filtering (Ruckebusch, 1983) was used in the geochemical processing at sea to minimize statistical uncertainties in the logs, which can otherwise create erroneous negative values and anti-correlations (especially between Th and U). An alpha filter has been introduced more recently and is now recommended by Schlumberger for shore-based processing. This filter strongly smooths the raw spectral counts but keeps the total gamma-ray curve unsmoothed before calculating out the Th, U, and K. The outputs of this program are K (wet wt%), U (ppm), and Th (ppm), as well as total gamma-ray and computed gamma-ray (total gamma ray minus U contribution).

Step 4: Calculation of Al Concentration

The fourth processing routine calculates the concentration of Al in the formation using four energy windows recorded on the AACT. During this step, corrections are made for natural radioactivity, bore-hole-fluid neutron-capture cross section, formation neutron-capture cross section, formation slowing-down length, and borehole size.

Porosity and density logs are needed as inputs into this routine to convert the wet-weight percentages of K and Al curves to dry-weight percentages. A porosity log was calculated from the deep induction log collected at Site 906 using the relationship of Archie (1942). After comparison with shipboard core measurements the final porosity curve used in the processing consisted of interpolated core measurements in the lower portion of Hole 906A spliced with the resistivity-derived porosity above 372 mbsf.

A correction was also made for Si interference with Al; the ^{252}Cf source activates the Si, producing the aluminum isotope, ^{28}Al (Hertzog et al., 1989). The program uses the Si yield from the GST to determine the Si background correction. The program outputs dry-weight percentages of Al and K, which are combined in the next processing step with the GST-derived elemental yields in the oxide closure model.

Step 5: Normalization of Elemental Yields from the GST to Calculate the Elemental Weight Fractions

Relative concentrations of the GST-derived elemental yields can be determined by dividing each elemental yield by a relative spectral sensitivity factor (S_i). This factor is principally related to the thermal neutron-capture cross sections and also to its gamma-ray production and detection probability of each element (Hertzog, 1989). The relative elemental concentrations are related to the desired absolute concentrations by a depth-dependent normalization factor (F), as defined by the relationship:

$$Wt_i = FY_i/S_i, \tag{4}$$

where

Wt_i = absolute elemental concentration and
Y_i = relative elemental yield.

The normalization factor is calculated on the basis that the sum of all the elemental weight fractions is unity (100%). The closure model handles the absence of carbon and oxygen, which are not measured by this tool string, with the approximation that each of the measurable elements combines with a known oxide or carbonate. The dry weight percent of Al and K are normalized with the reconstructed elemental yields to determine the normalization factor at each depth interval from the following equation:

$$F(\Sigma_i X_i Y_i/S_i) + X_K Wt_K + X_{Al} Wt_{Al} = 100, \tag{5}$$

where

X_i = oxide factor (atomic wt of the associated oxide or carbonate of element i ÷ atomic wt of element i);
X_K = oxide factor (atomic wt K_2O ÷ atomic wt of K);
Wt_K = dry wt% of K as determined from the NGT;
X_{Al} = oxide factor (atomic wt of Al_2O_3 ÷ atomic wt of Al); and
Wt_{Al} = dry wt% of Al as determined from the AACT.

The value X_i accounts for the C and O associated with each element. Table 9 lists the oxide factors used in this calculation for Hole 906A.

Step 6: Calculation of Oxide Percentages

This routine converts the elemental weight percentages into oxide percentages by multiplying each by its associated oxide factor, as

shown in Table 9. Shipboard carbonate measurements of core samples have been converted into CaO for comparison to the GST-derived CaO.

Step 7: Calculation of Error Logs

The calculated statistical uncertainty of each element is calculated for each of the elements measured with the GST and NGT (Grau et al., 1990; Schweitzer et al., 1988). This error is strongly related to the normalization factor, which is calculated at each depth level (Eq. 5). The normalization factor is usually displayed along with the log measurements. A lower normalization factor represents better counting statistics and therefore higher quality data.

Synthetic Seismograms

Synthetic seismograms are generated from an impedance log. The interval transit time log (from the DSI and SDT tools) and the density log (from the HLDT tool) are used to generate an impedance log (Gal'perin, 1974). The impedance vs. depth log is then converted to impedance vs. two-way traveltime and convolved with a zero-phase Ricker wavelet or other digitized wavelets representative of the source used to generate the original seismic profile. Digital waveforms of the seafloor reflection recorded during the Leg 150 Site Survey (cruise Ew9009; Mountain and Miller, 1991) approximate the source waveform for key profiles across drill sites and were also used to construct synthetic seismograms. The vertical resolution of a 30-Hz wavelet is about 15–30 m (depending on interval velocity), so reflecting surfaces less that 8–15 m apart can rarely be distinguished as separate reflectors. The final synthetic seismogram calculated includes interbed multiples.

SEISMIC STRATIGRAPHY

Seismic stratigraphic studies of the Leg 150 region began with data collected by the USGS in the 1970s (e.g., multichannel seismic [MCS] Line 25; Grow et al., 1979) (see Fig. 1 in Chapter 1, this volume). In 1990, Exxon Production Research (EPR) released several shelf-slope MCS profiles (see Fig. 2 in Chapter 2, this volume) in a workshop attended by workers from EPR, Rutgers, and LDEO (Greenlee et al., 1992). Sequence boundaries on these profiles were recognized on the basis of regional unconformities identified by top-discordant (toplap and erosional truncation) and base-discordant (onlap and downlap) seismic reflector geometries (Mitchum et al., 1977). The reflectors were loop correlated around the Exxon grid (see Fig. 2 in Chapter 2, this volume). The sequence boundaries identified were related to those of Greenlee et al. (1988), who correlated them to the Haq et al. (1987) inferred global sea-level record (see Fig. 5 in Chapter 2, this volume). The ages of the sequences were reevaluated (Greenlee et al., 1992), and the data used to plan MCS and SCS surveys by the *Maurice Ewing* in 1990 (see Figs. 3 and 4 in Chapter 2, this volume).

We collected 3700 km of seismic data on cruise Ew9009 in November, 1990 (see Figs. 3 and 7 in Chapter 2, this volume). Two-thirds of these profiles are 120-channel, tuned air-gun-array data across the shelf that complement the Exxon data and tie to industry wells (see Fig. 3 in Chapter 2, this volume); the rest are single-channel, water-gun data on the upper continental slope (see Fig. 7 in Chapter 2, this volume). These seismic profiles tie the shelf stratigraphy to a number of boreholes drilled previously, to outcrop samples collected by the *Alvin* in 1989 (W.B.F. Ryan and K.G. Miller, unpubl. data, 1989), and to Leg 150 boreholes. The new profiles represent a clear improvement in resolution over older seismic data, caused in part by our using a tuned air-gun array (six guns totaling 1350 in.[3]), shallow towing depths (20 ft.), short streamer group lengths (12.5 m), F-K filtering to minimize water column reverberations, and our deliberate efforts to preserve seismic images of shallow, fine-scale stratal geometry dur-

Table 9. Oxide factors used in normalizing elements to 100% and converting elements to oxides.

Element	Oxide/carbonate	Conversion factor
Si	SiO_2	2.139
Ca	CaO	1.399
Fe	FeO*	1.358
K	K_2O	1.205
Ti	TiO_2	1.668
Al	Al_2O_3	1.889
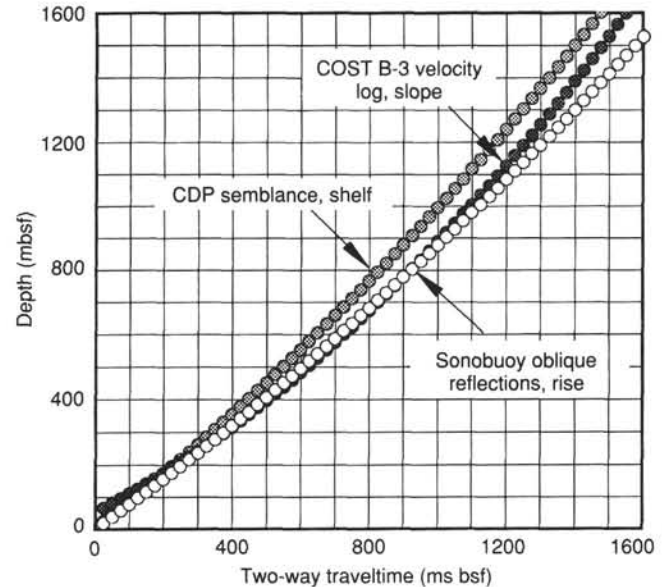
Figure 10. Time-depth relationships derived from three types of sound velocity measurements performed in the vicinity of Leg 150 drilling (see text for details).

ing all stages of acquisition and processing. All Ew9009 profiles are displayed with black representing negative acoustic pulses. Wherever possible, reflectors were traced as the top edge of strongly negative (i.e., black) wavelets.

The interpretation of Ew9009 seismic data began with identifying the several "Icehouse" (Oligocene-Miocene) sequence boundaries previously identified in the Exxon grid. Vertical resolution in the Ew9009 profiles is on the order of 15 to 20 m down to several hundred meters below seafloor, and we were able to detect two and sometimes more seismic discontinuities between sequence boundaries seen on the Exxon lines. Not all of these surfaces are unequivocally related to changes in relative sea level; they could instead be local expressions of lobe switching and marine onlap, although the major sequence boundaries seen in the Exxon lines show regional consistency that cannot be attributed to local processes (Greenlee et al., 1988, 1992). Nonetheless, loop correlations support as many as eight "candidate" Miocene sequence boundaries in addition to the previously identified four between 10 and 17 Ma (Greenlee et al., 1992; see Fig. 6 in Chapter 2, this volume).

We traced seismic reflectors from the continental shelf to the slope using the Ew9009 seismic grid, including the following Oligocene-Miocene reflectors of Greenlee et al. (1992): Red, Tuscan, Yellow-2, Pink-2, and Green. We also traced the informal ochre, sand, true blue, pink-3, and green-2 reflectors of G.S. Mountain, K.G. Miller, and N. Christie-Blick (unpubl. data, 1990) (see Fig. 1 in Chapter 2, this volume). In addition, we named several new reflectors correlated on the Ew9009 profiles examined during Leg 150 and confirmed by seismic profiles collected during the leg (see Chapter 4, this volume). How-

Table 10. Tentative correlations of seismic reflectors, New Jersey continental slope, Leg 150.

Informal name (Leg 150)	Color	Correlation	Series
p1	yellow	Oxygen isotope stage 7/6 transition[a]	middle Pleistocene
p2	blue	Oxygen isotope stage 9/8 transition[a]	middle Pleistocene
p3	green	Oxygen isotope stage 10 hiatus; stage 11/10 transition[a]	middle Pleistocene
p4	purple	Oxygen isotope stage12.4/12.3 transition[a]	middle Pleistocene
p5	orange	Oxygen isotope stage 13/12 transition[a]	middle Pleistocene
p6	indigo	Disconformity separating stage 15[a] and upper Pliocene	middle Pleistocene/upper Pliocene
m0.3	yellow	Near base of C4n	middle upper Miocene
m0.5[b]	Red	C4Ar?	middle upper Miocene
m0.7	blue	Below is C4Ar?	lower upper Miocene
m1[b]	Tuscan	C5r?	upper middle Miocene
m1.5[c]	orange	C5r?	upper middle Miocene
m2[b]	Yellow-2	C5Ar?	upper middle Miocene
m3[b]	Blue	Older than C5Ar, NN7, and FO *G. fohsi fohsi*	middle middle Miocene
m4[b]	Pink-2	?Near NN5/NN6 boundary	middle middle Miocene
m5[b]	Green	Near Zone NN4/NN5 boundary; possibly upper NN4	near lower/middle Miocene boundary
m5.2[c]	ochre	?Unconformity NN2/NN4?	lower Miocene
m5.4[c]	sand	Within Zone NN2	lower Miocene
m5.6[c]	true blue	Within Zone NN2	lower Miocene
m6[c]	pink-3	Unconformity NN2/NP25	near Oligocene/Miocene boundary
o1[c]	green-2	Unconformity NP23/NP19-20	middle Oligocene/upper Eocene
e1	yellow	Unconformity NP16/NP19-20	middle/upper Eocene boundary
e2[c]	red-3	Middle part of Zone NP15	top lower middle Eocene porcellanites

[a]Based on GRAPE and magnetic susceptibility correlations to SPECMAP oxygen isotope time scale.
[b]Possibly equivalent to the shelf reflectors of this color (Greenlee et al., 1992).
[c]Possibly equivalent to the shelf reflectors of this color (G.S. Mountain, K.G. Miller, and N. Christie-Blick, unpubl. data, 1990).

ever, there are uncertainties in some correlations of the shelf reflections because of problems with downlapping, erosion, and masking of reflectors. Therefore, we established a local alphanumeric scheme that is tentatively correlated with the shelf reflections (Table 10).

Time-depth (t-d) relationships for correlation of seismic profiles to the slope boreholes were initially derived from three sources (Fig. 10): (1) a velocity log from the COST B-3 well (Scholle, 1980); (2) shelf semblance velocities obtained from analysis of Ew9009 cdp stacks on the adjacent shelf (G.S. Mountain, unpubl. data, 1991); and (3) sonobuoy data from the continental rise (Houtz and Ewing, 1974; Mountain and Tucholke, 1985). In general, the COST B-3 sonic velocities provided the most reasonable correlations between seismic profiles and cores, although they are not applicable above the first sonic velocity measurement made at the well (~329 mbsf). None of the t-d functions yielded realistic velocities for the section within 40 milliseconds (ms) of the seafloor. We modified these t-d relationships using seismic-borehole correlations made at Site 902 (see "Seismic Stratigraphy" section, Chapter 6, this volume). We took the two-way traveltimes (TWT) and depth (mbsf) of the most prominent reflectors at Site 902 (see Table 16 in Chapter 6, this volume) and fitted a second-order polynomial to the data. This polynomial function was used to predict the sub-bottom depth of reflectors traced to Sites 903, 904, and 906. The predicted sub-bottom depth proved to be remarkably accurate at Site 903 (maximum 3% offset from correlations determined below) but less accurate at Sites 904 and 906.

Ms 150IR-103